Kusky, T., Wang, L., Robinson, P. T., Huang, Y., Wirth, R., Ning, W., Zhong, Y., Polat, A. (2021): Ultra-high pressure inclusion in Archean ophiolitic podiform chromitite in mélange block suggests deep subduction on early Earth. - Precambrian Research, 362, 106318.

https://doi.org/10.1016/j.precamres.2021.106318

Ultra-high pressure inclusion in Archean ophiolitic podiform chromitite in mélange block suggests deep subduction on early Earth

Timothy Kusky[a,b*], Lu Wang[a*], Paul T. Robinson[a], Yang Huang[a], Richard Wirth[c], Wenbin Ning[a], Yating Zhong[a] & Ali Polat[a,d]

[a]State Key Laboratory of Geological Processes and Mineral Resources, Center for Global Tectonics, School of Earth Sciences, China University of Geosciences, Wuhan 430074, China.

[b]Three Gorges Research Center for Geo-hazards, China University of Geosciences, Wuhan 430074, China.

[c] Helmholtz Center Potsdam German Research Centre for Geosciences GFZ, D-14473 Potsdam, Germany.

[d]School of the Environment, University of Windsor, Windsor, ON N9B 3P4, Canada.

ABSTRACT

The discovery of ultrahigh pressure (UHP) minerals in orogenic belts has revolutionized our understanding of subduction and the return flow of previously deeply subducted material to Earth's surface as part of the cycling and interaction of crustal and mantle systems. One class of UHP minerals is found as inclusions in orogenic peridotite-hosted podiform-chromite systems, within Phanerozoic ophiolites and ophiolitic mélanges. Such inclusions have opened a window into processes of recycling of crustal materials to the deep mantle and back through subduction and mantle convection in Phanerozoic orogens. Here, we document the first occurrence of an

UHP mineral hosted in an ophiolitic podiform chromitite mélange from the Neoarchean paired metamorphic belt of the Central (Taihang) Orogenic Belt, Northern China. Numerous inclusions of rutile, apatite, dolomite, and amphibole are interpreted to be crustal-derived; they occur in podiform chromite grains hosted in a 2.6-2.5 Ga ophiolitic mélange now part of the North China Craton and formed by subduction of oceanic and continental material. Microstructures and phase relationships in a multi-phase inclusion of TiO_2(II), rutile, apatite, and tremolite yield minimum P-T conditions of 7.5 GPa at 1000°C, indicating that the crustal host, including carbonates, were subducted to depths > 270 km, transferred to the mantle of the overriding plate, and returned to the surface by 2.5 Ga. We suggest that slab rollback forced upward mantle flow, incorporating entities from the lower plate, perhaps in serpentinite diapirs, resulting in adiabatic melting that allowed crustal material to be trapped in chromite grains crystallizing in high-Mg melts. Contrasting bulk moduli and thermal contraction of the inclusions and host chromite protected the inclusions from P-induced back-reaction during exhumation. Together, these features show that the 1600 km long Central (Taihang) Orogenic Belt is emerging as the world's first well-documented Phanerozoic style orogen, with classic tectonic zonation, ophiolitic mélanges, paired metamorphism, local evidence for UHP conditions, foreland basins, and late to post orogenic magmatism. Applying the null hypothesis, we explain this high degree of similarity by invoking the operation of Phanerozoic style plate tectonics, at least throughout the 1600 km length of the COB, and by geological comparison, in other similar aged geological terrains globally. From this we infer modern-style plate tectonics was operating in the Neoarchean.

Citation: Kusky, T.M., Huang, Y., Wang, L., Robinson, P., Wirth, R., Ning, W., Wang, J., Deng, H., Zhong, Y., and Polat, A., Ultra-high pressure inclusion in Archean ophiolitic podiform chromitite in mélange block suggests deep subduction on early Earth, **Precambrian Research,** 106318

Keywords

Archean; subduction; ultrahigh pressure metamorphism; deep carbon cycle; North China Craton

Graphical abstract

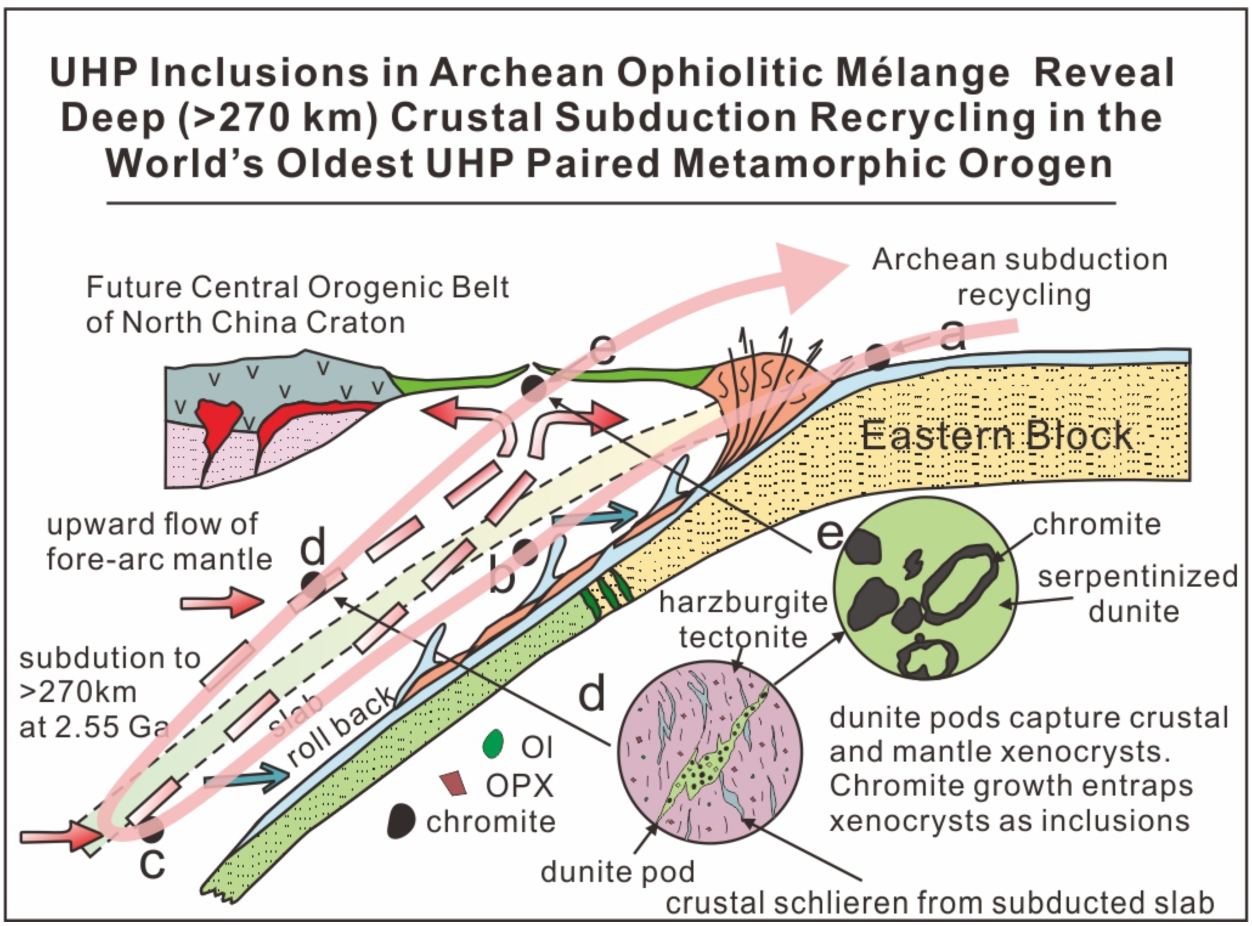

Highlights

- Ultra-high pressure TiO_2 II identified in Archean ophiolitic podiform chromite mélange
- Crustal minerals subducted to >270 km at 2.55 Ga, then recycled to surface
- UHP mélange is part of paired metamorphic Central (Taihang) Orogenic Belt of North China
- Data shows operation of subduction-related deep carbon cycle in Archean
- Convergent margin processes in Archean were similar to those of Phanerozoic

---

1. Introduction

One of the most controversial issues in Earth and Planetary Sciences today is determining when the style of modern plate tectonics developed on Earth, and for how long the subduction-driven, life-sustaining deep carbon cycle has been in operation (National Academies of Sciences, 2020). Field-based structural, petrological, sedimentological, and geochemical evidence is consistent with modern style tectonics operating since the Eoarchaean (Harrison, 2009; Polat, 2012; Kusky et al., 2018; Windley et al., 2021) or Mesoarchaean (Cawood et al., 2018), but some have argued that the metamorphic record is not consistent with modern style tectonics, because of the absence of paired metamorphism (low *dT/dP* with high *dT/dP*) and orogenic ultra-high pressure (UHP) minerals in Archean orogenic belts (c.f. Stern, 2008; Brown and Johnson, 2019; Zheng and Zhao, 2020; Kusky, 2020). Recent studies have shown that the Central (Taihang) Orogenic Belt (COB) of the North China Craton (NCC) contains geological records of a late Archean arc/continental collision, that includes hallmark features of Phanerozoic collisional orogens including accretionary wedges with accreted ocean plate stratigraphy, ophiolitic mélanges, fore-arc ophiolites, supra-subuduction zone magmatic systems, sea-floor hydrothermal systems, zones of Alpine-style nappes, a hinterland of high-grade metamorphic and magmatic rocks, and foreland basins filled contemporaneously with late stages of collision (Kusky et al., 2016, 2020; Deng et al., 2018; Wang et al., 2019; Huang et al., 2019; Peng et al., 2020; Ning et al., 2020; Jiang et al., 2020). Most recently the COB has been shown to contain a clear record of late Archean spatially and temporally linked paired metamorphism (low-medium dT/dP with high dT/dP) associated with this collision (Huang et al., 2020), which is one of the diagnostic indicators of plate tectonics in old rocks (Brown and Johnson, 2019).

UHP minerals (> 2.7 GPa, the pressure needed to stabilize coesite) have been documented in young orogens from about twenty localities around the world (Hacker and Gerya, 2013; Gilotti, 2013; Gonzalez et al, 2020), resulting in a paradigm shift in understanding how deeply continental and oceanic crustal material can be subducted, then returned to the surface. Some very significant developments in this field demonstrate that continental and oceanic material can be subducted to depths exceeding 150 km, and then returned to the surface in UHP orogenic belts (Hacker et al., 2013; Wang et al., 2014; Xia et al., 2018; Gonzalez et al., 2020). However, to-date, no orogenic UHP rocks have been discovered in Archean orogens.

UHP inclusions in chromites from podiform chromitites have been documented in ophiolites throughout the Phanerozoic (Dobrzhinetskaya et al., 2009; Robinson et al., 2015; Yang et al., 2007, 2014; Zhou et al., 2014; González-Jiménez et al., 2017; Lian et al., 2020) and represent windows into the P-T-t conditions operating on Earth. They have led to numerous models involving interaction of subducted lithosphere, deep mantle convection, and return of old crustal material to be preserved within younger oceanic lithosphere (Robinson et al., 2015; González-Jiménez et al., 2017; Lian et al., 2020). We report the first unambiguous occurrence of an UHP mineral from an inclusion in chromite from a podiform chromitite block in a well-characterized Neoarchean ophiolitic mélange (Li et al., 2002; Kusky et al., 2016; 2020; Wang et al., 2019; Ning et al., 2020; Huang et al., 2021). We interpret this result to relate to plate tectonic processes that must have operated before 2.5 Ga and is significant for characterizing plate tectonic processes on early Earth, constraining the minimum depths of subduction, and tracking the interaction of surface tectonic-and deep mantle convective-recycling processes through deep time.

2. Geological background

Ophiolites and ophiolitic mélanges are both tectonic indicators of sutures where oceans have closed through subduction and collision (Festa et al., 2019; Kusky et al., 2018, 2020). The Zunhua ophiolitic mélange is a key component of the Central (Taihang) Orogenic Belt (COB) that separates the Eastern and Western Blocks of the NCC (Fig. 1a; Kusky et al., 2016, 2020). The mélange is composed of strongly deformed metasedimentary rocks (biotite-plagioclase-quartz (BPQ) gneiss), with structurally included blocks that show a strong affinity to rocks of the modern oceanic realm (Fig. 1b). These exotic mafic-ultramafic blocks include meta- pillow basalt, gabbro, pyroxenite, harzburgite and dunite, and podiform chromitites are common in dunite pods within the harzburgite blocks (Li et al., 2002; Huang et al., 2004; Kusky et al., 2004, 2007, 2016, 2020;Wang et al., 2019). Together with lenticular structural slices of Banded Iron Formation (BIF) (submarine volcanogenic exhalative deposits), the map patterns and structural relationships (Fig. 1b) are indistinguishable from those of typical modern ophiolitic mélanges (Kusky et al., 2020). The most abundant mineral of the chromitite-bearing dunites and harzburgites is serpentine, with lesser amounts of chromite, talc, and magnesite accompanied by minor olivine (Ning et al., 2020). Thus, nearly all primary minerals of the host harzburgites and dunites have been altered to serpentine. However, mineral inclusions are found in the chromites and may preserve primary compositions if armoured by their host.

Most of the podiform chromite bodies at Zunhua are small, between 0.5-2 m thick, 1-2 m long, and extend up to 30 m in depth (Figs. 1c-f). Some however are larger, exceeding 100 meters in length, and have been extensively mined (Kusky et al., 2007). Most of the larger bodies form irregular lenses of dunite including chromite in pod-like bodies in the host serpentinized harzburgite blocks (Fig. 1e), and within some of the pods, some of the chromites form igneous layers that locally show grading, magmatic folds, and asymmetric fabrics indicative of flow (Li et al., 2002; Huang et al., 2004; Kusky et al., 2007). Chromite layers within the pods are typically 1-2 cm thick, alternating with 10-50 cm thick dunite layers. The chromites have disseminated, nodular and orbicular textures that locally form cumulate layers within small magma chambers defined by the dunite pods (Huang et al., 2004). In addition to these chromites, the host harzburgite foliations are cut by thin veins of chromite with dunitic rims (Figs. 1g, h), suggesting a melt-host harzburgite reaction may have left residual chromite-dunite as pods (Li et al., 2002; Kusky et al., 2007). Ning et al. (2020) and Huang et al. (2021) show that the chromite has chemical signatures indicating that the infiltrating melt was Mg-rich, and likely boninitic.

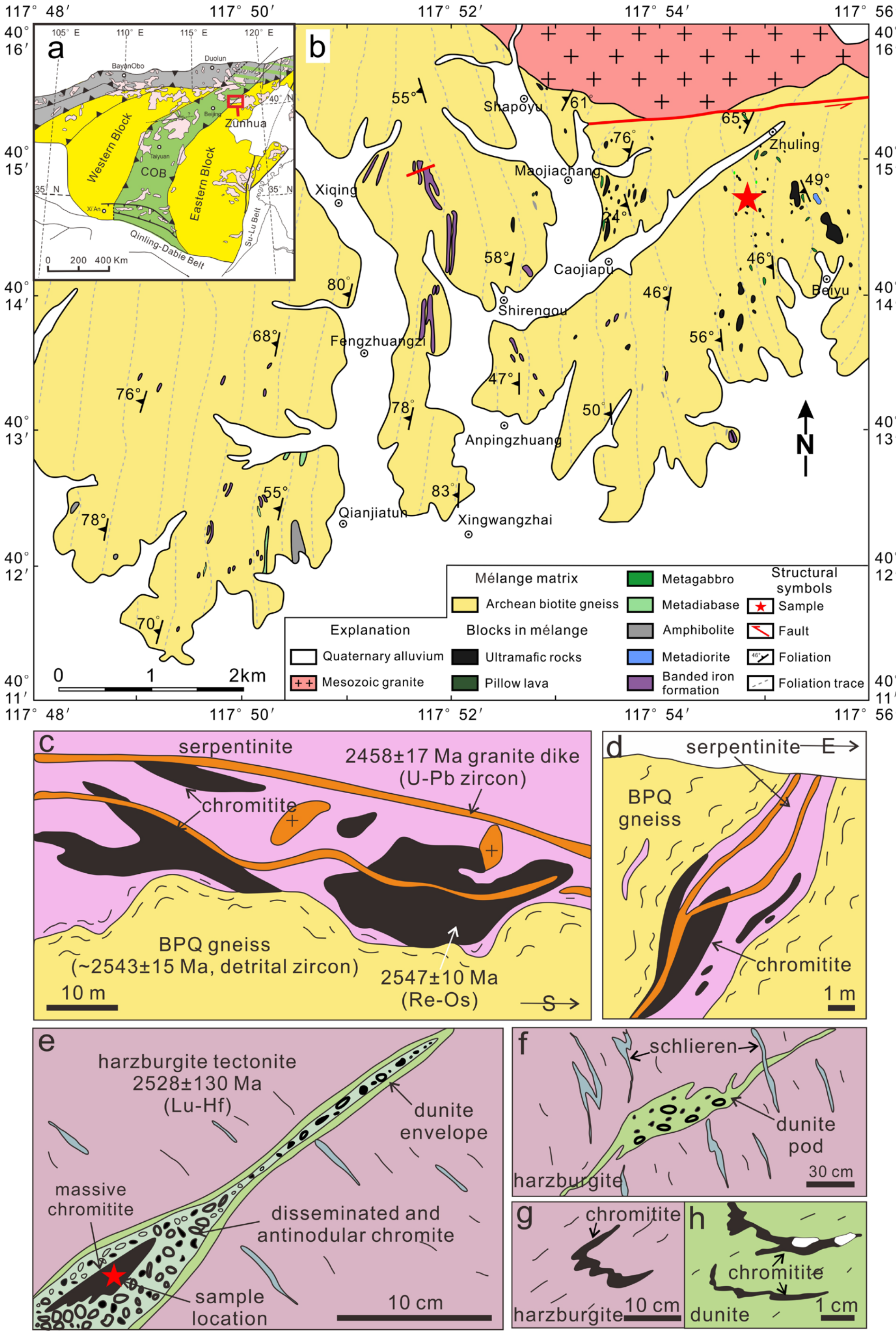

Fig.1. Maps and outcrop sketches showing important geological relationships in the study area. (a) Tectonic map showing the division of North China Craton (NCC) into the Eastern and Western Blocks, separated by the Central (Taihang) Orogenic Belt (COB), and the location of the study area (after Kusky et al., 2016). (b) Detailed geological map of the study area (mapping by the authors: Wang et al., 2019; Ning et al., 2020). The podiform chromitites

occur in blocks of serpentinized harzburgite tectonite and rare lherzolite (grouped as ultramafic rocks in legend). (c)-(h) Outcrop sketches of key relationships from map area of Fig. 1b. (c) Outcrop map and (d) cross section of the Maojiachang podiform chromite block (e) pod of chromite-bearing dunite cutting mantle tectonite fabric in harzburgite at Zhuling, showing a rim of dunite, and internal zones of disseminated and antinodular chromite, and massive chromitite, Red star shows location of sample with UHP inclusion. (f) dunite pods with disseminated chromite cutting mantle harzburgite tectonite with schlieren at Zhuling, (g) chromitite vein with dunitic envelope cutting harzburgite at Zhuling, (h) chromitite vein within serpentinized dunite at Zhuling. Outcrop sketches c-h modified after Huang et al., (2004). Outcrop TK-NCC-2002-580 is from the Zhuling body (location: N 40 14.739; E 117 54.794), from which sample (massive chromitite, MC-20, see panel e) containing the UHP TiO_2 II inclusion was taken from the position shown in panel e.

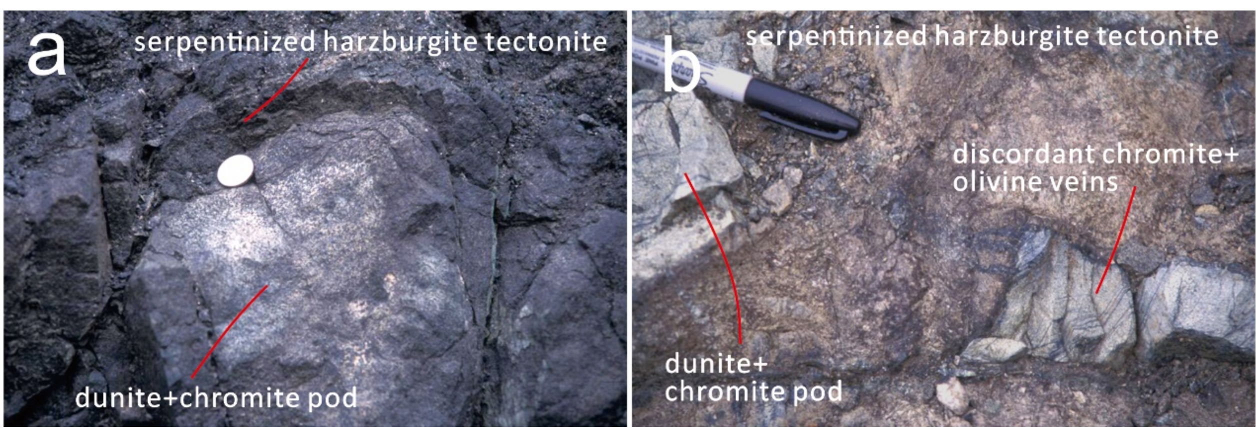

Fig. 2. (a) Chromite pod with disseminated chromite surrounded by strongly foliated harzburgite tectonite; (b) chromitite in dunite in tabular pod in sheared serpentinized harzburgite, cut by thin discordant veins of chromitite with dunitic rims.

Podiform chromitites are only known to form in supra-subduction zone ophiolites (Li et al., 2002; Kusky et al., 2007). Those in the Zunhua ophiolitic mélangeare hosted in dunite pods within harzburgites and show disseminated, massive, nodular and orbicular textures (Figs. 2, 3), clearly meeting the definition of typical ophiolitic podiform chromitites (Thayer, 1964).

Moreover, the mineral chemistry and platinum group element (PGE) geochemistry of the Zunhua chromitites (Kusky et al., 2007; Ning et al., 2020; Huang et al., 2021) are also similar to those of well-known Phanerozoic podiform chromitites worldwide (Zhou, 2005; Arai and Ahmed, 2017). Outcrop-scale structures show high-temperature deformation in schlieren and chromite-mylonites, whereas microstructural studies of the Zunhua chromites (Li et al., 2002; Huang et al., 2004; Polat et al., 2006; Kusky et al., 2007) documented high-temperature grain boundary pull-aparts, preferred crystallographic slip on (010)[100] slip systems in olivine inclusions, asymmetric recrystallized tails on orthopyroxene porphyroclasts, high-temperature deformation bands in inclusions in olivine, and used established paleothermometers (Holtzman, 2000; Nicolas, 1989; Nicolas and Azri, 1991), to estimate the crystallization temperatures of the chromite to have been between 1000 °C and 1250°C, consistent with recent high-pressure experimental work (Raterron et a., 2012; Wang et al., 2017; Wallis et al., 2019).

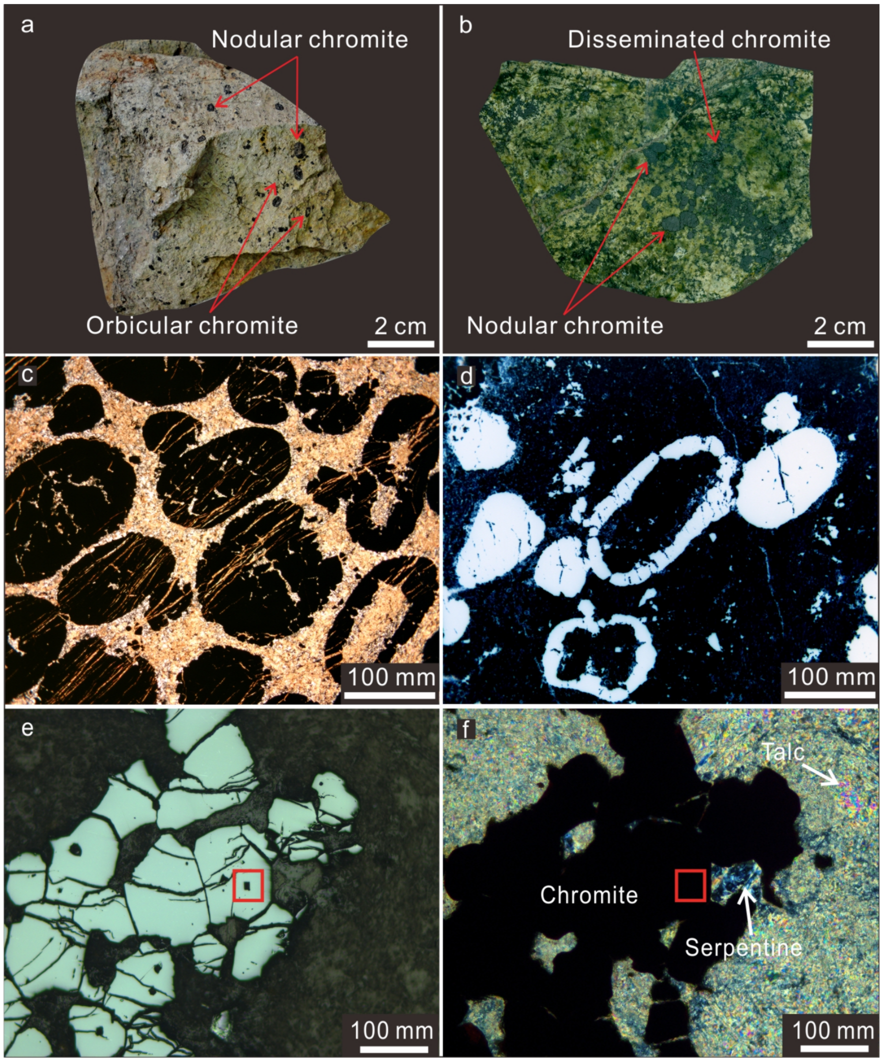

Fig. 3. Photographs of nodular and orbicular textures of podiform chromitite from the Zunhua ophiolitic mélange at Zhuling (Fig. 1b). (a) Hand specimen picture showing nodular chromites. (b) Scanning image of rock sample showing chromites with nodular and disseminated textures. (c) Photomicrograph of a thin section showing nodular and orbicular chromites (plane polarized light). (d) Photomicrograph of a thin section showing nodular and orbicular chromites (reflected light). (e) Reflected light photomicrograph of the massive chromite band from the Zhuling podiform location (TK-2002-NCC-580, thin section MC20). Red square indicates the FIB foil cutting position of the TiO_2 II bearing chromite grain. (f) Thin section photomicrograph of the same area as (e) in cross-polarized light. Figs.2e and 2f show the same position and viewing range, but with different light sources, causing slightly different appearance of the chromite grains.

Age constraints on the formation of the mélange, the blocks contained therein, and of the chromite grains are described in detail in W.B. Ning et al. (2020) and J.P. Wang et al. (2019), and briefly summarized here (Fig. 4). Blocks in the Zunhua mélange have all yielded ages greater than 2.5 Ga, with most, using various methods and multiple labs, falling between 2.55 and 2.52 Ga (review in Kusky et al., 2020). These ages include detrital zircons from magnetite quartzite blocks and lenses (2541-2553 Ma; Zhang et al., 2012), and $^{207}Pb/^{206}Pb$ zircon ages from blocks of gabbro ranging from 2.51-2.55 Ga (Kusky et al., 2020; Wang et al., 2019; Kusky et al., 2016) and Lu/Hf ages on blocks of peridotite of 2528 +/- 130 Ma (Polat et al., 2006). Detrital zircons analyzed from the metasedimentary matrix of the mélange (BPQ gneiss) yield age peaks between 2522 to 2633 Ma, and the youngest detrital zircon has an age of 2522 +/- 32 Ma (Wang et al., 2019). Statistically the youngest group of detrital zircons (n=29) yields a weighted mean $^{207}Pb/^{206}Pb$ age of 2543 +/- 15 Ma (Ning et al. 2020), which we take as the maximum depositional age. Metamorphic rims on the detrital zircons from different sample sets yield a weighted means $^{207}Pb/^{206}Pb$ age of 2467 +/- 27 Ma (Wang et al., 2019), and 2481 +/- 32 Ma (Ning et al., 2020), within error of each other. Undeformed syenogranite dikes that cut the foliation in the mélange have yielded ages of 2458 +/- 17 Ma (Wang et al., 2019). The syenogranite, and metamorphic rims of the zircons all broadly overlap in age, and are associated with cross-cutting quartz veins, which have also yielded indistinguishable $^{207}Pb/^{206}Pb$ ages of 2466 +/- 12 Ma (Wang et al., 2019).

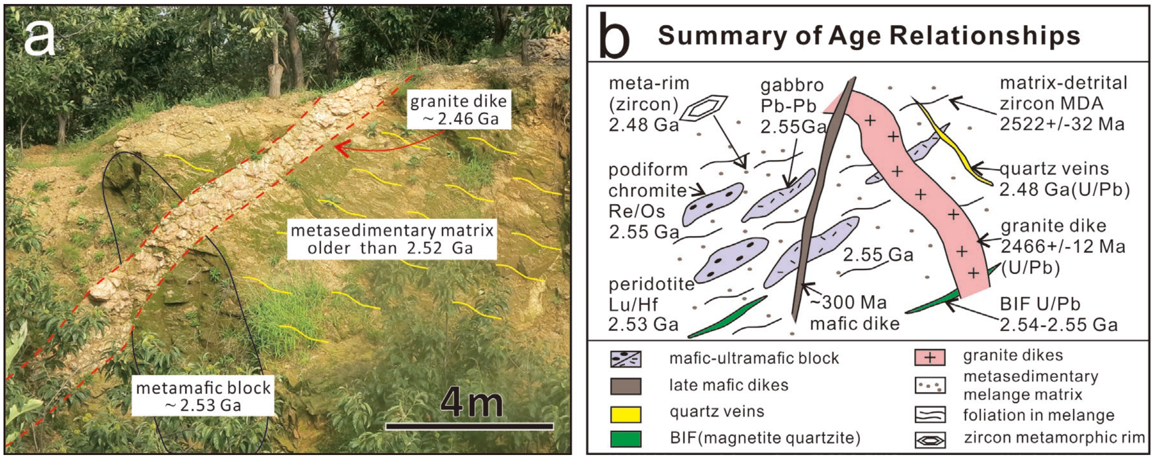

Fig. 4. (a) Outcrop photo showing 2.46 Ga undeformed granitic dike, cutting circa 2.53 Ga mafic block, in a metasedimentary mélange matrix with an age > 2.52 Ga. (b) Schematic diagram summarizing the cross-cutting relationships and ages determined from multiple methods that demonstrate the Archean age of the Zunhua ophiolitic mélange and contained ophiolitic podiform chromitites.

Of particular interest are the Re-Os range of the chromite grains, which were dated in two different labs (Carnegie, DTM in Washington D.C., and University of Science and Technology of China), with the result being an average Re-Os age of 2547 +/- 10 Ma for all the chromite grains analyzed (Kusky et al., 2007). However, since these results did not yield a well-constrained isochron, the individual model ages need to be considered since it is possible that there may be chromites or material of different ages or sources recycled from the deep mantle in the chromite deposits. With that in mind, we note that the model ages reported by Kusky et al. (2007) have one group that clusters around 2.5 Ga (within errors), and a few model age determinations that are clustered around 2.65-2.72 Ga. They report the best data from three massive chromitites (with Os> 300 ppb) yields chondritic osmium isotopic composition for the mantle at 2.6 Ga, of 0.110126 +/- 0.00004.

Taken together, the data indicates the mélange formed between 2.55 and 2.52 Ga, incorporates some older material, and metamorphic effects of the collision of the arc and continent lasted until

2.48-2.46 Ga (Kusky et al., 2020). The ages of the chromite grains is generally the same as the ages of the host peridotites and their derived melts, but a possibility that awaits further testing is whether there may be an older age population of chromite grains within the sample set.

3. Methods

3.1. Mapping and Sample collection

Samples were collected in the field during detailed structural mapping of the area shown in Fig. 1b.Outcrop sketches and detailed sample locations are shown on Fig. 1c-g. Methods used for mapping (Li et al., 2002; Huang et al., 2004; Kusky et al., 2007; Wang et al., 2019), structural analysis (Li et al., 2002; Huang et al., 2004; Kusky et al., 2007), geochronology (Kusky et al., 2007; Polat et al., 2006; Wang et al., 2019; Ning et al., 2020), geochemistry (Ning et al., 2020; Huang et al., 2021), paleo-thermometry (Li et al., 2002), and petrography (Huang et al., 2004; Ning et al., 2020) are described in the cited papers above. Specialized techniques used in this work include Scanning Electron Microscopy (SEM), Focused Ion Beam (FIB) milling, and Transmission Electron Microscopy (TEM). Detailed analytical procedures are described in supplementary text S1 "Analytical Methods."

4. Results

4.1.Trapping of mineral inclusions in chromite grains

Figure 5 shows textural relationships which with geochemical and other data (Ning et al., 2020; Huang et al., 2021) we use to propose a petrogenetic model in which an olivine-saturated melt (boninite) derived from partial melting above a slab reacted with orthopyroxene in depleted harzburgite of the mantle wedge to produce replacive dunite pods containing chromite. The dynamic flow of a hydrous melt in the initial dikes in lead to formation of nodular and orbicular chromite initially as disseminated immiscible blobs, that formed inward-growing orbicules (Fig. 5) then nodules that trapped host minerals and liquids. Eventually, the nodules became concentrated by melts or formed cumulate layers depending on the dynamics of the flow of the early melts and replacive reactions.

Both single and multi-phase mineral inclusions within the Zunhua chromite grains include silicates, PGM (platinum group minerals), base metal sulfides, carbonates and others that are very similar to those found in Phanerozoic ophiolites (c.f. Dobrzhinetskaya et al., 2009; Robinson et al., 2015; Yang et al., 2007, 2014; Zhou et al., 2014). The most common single-phase inclusions are Os-Ir PGM and silicates including olivine, enstatite, diopside and tremolite (Table 1). Multi-phase inclusions include various combinations of silicate minerals, along with apatite and rutile. Carbonate minerals, particularly dolomite, are surprisingly abundant, and some native elements, such as Os and C are present (Table 1). Thus, some of the inclusions appear to be derived from the host mantle (e.g., olivine and enstatite were likely derived from harzburgite), whereas others (tremolite, apatite, carbonates, etc.) were likely derived from crustal material, although some could possibly represent mantle-derived minerals as well. In younger ophiolites, similar suites of mineral inclusions are thought to have been included in chromite grains after partial assimilation of the remnants of subducted slabs and overlying sediments in the mantle (Yang et al., 2007; Zhou et al., 2014; González-Jiménez et al., 2017; Lian et al., 2020).

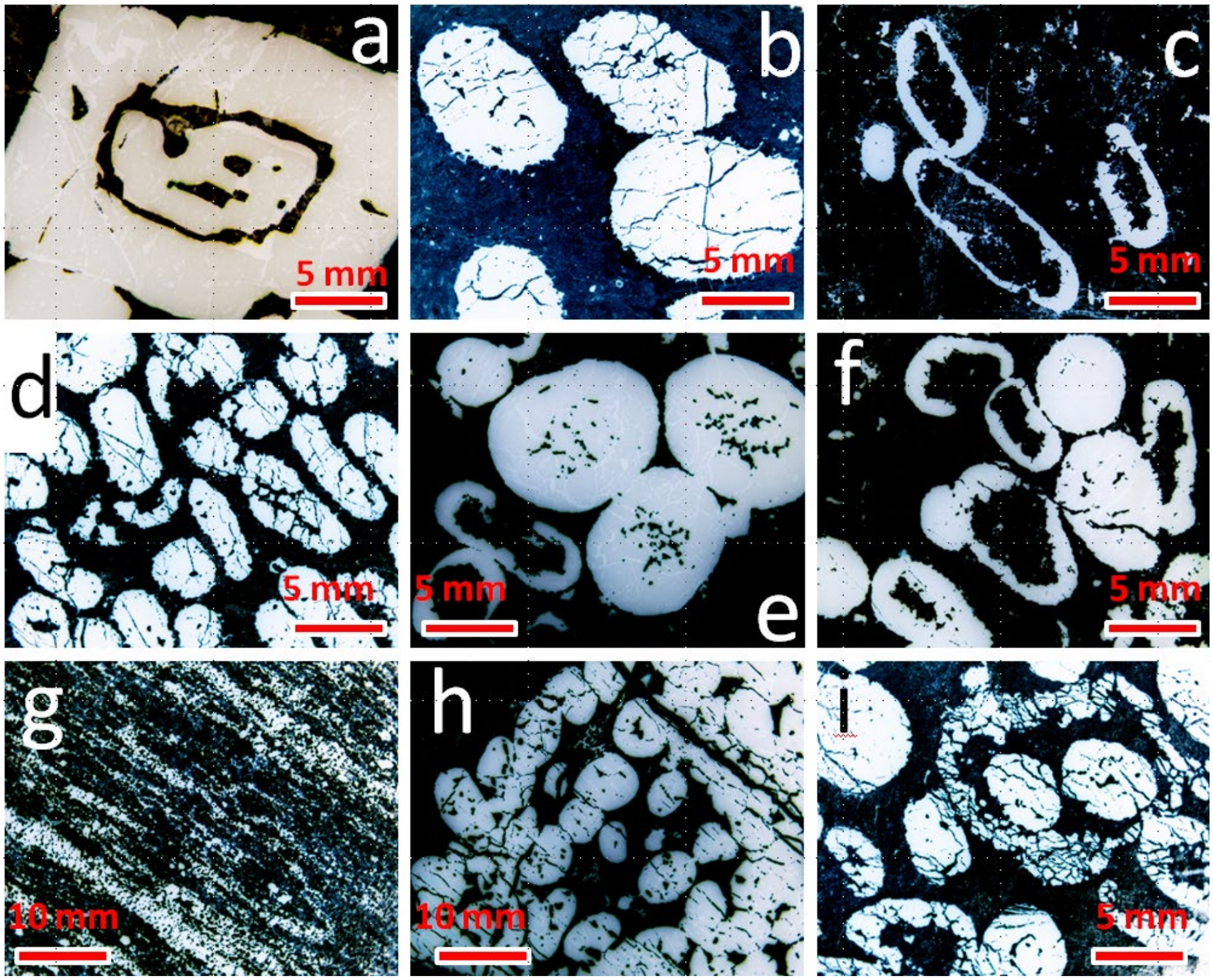

Fig.5. Typical microtextures of chromite grains in the Zunhua podiform chromitite bodies all taken in reflected light microscopy. The chromite grains are bright, and the faint brighter white lines in some of the grains are more-altered ferrit-chromite. The dark tones are serpentinizeddunite. (a) cubic grain of disseminated chromite. Note the ol-filled negative crystals defining the "happy face" in the center of the crystal; (b) nodular chromite grains with cracks, and small inclusions of the host dunite filling the negative cubic crystals; (c) orbicular chromite grains, with smooth outer rims, and irregular inner rims with areas showing negative crystal faces suggesting inward growth of chromite, capturing the host dunite in the cores; (d) nodular and semi-cubic chromite grains, some with inclusions of the host ol melt that became flattened to form apparent cumulate igneous layering; (e) nodular and orbicular chromite that grew inward from smaller grains, leaving a semi-open core. Note how the chromite grains are "stuck" together, suggesting melt bubbles coalescing in an immiscible fluid; (f) nodules and orbicules of chromite that accumulated in layers, with the impingement of grains breaking apart the fragile orbicules; (g) strongly deformed chromite

mylonite; (h) long strings of chromite nodules partially merged together that coalesced into a layer; (i) two nodules of chromite enclosed within an orbicular nest.

Inclusions in Zunhua Podiform Chromitites

Mineral species	Silicate		Ol, Di, Tr, Ph
	Base-metal mineral (BMM)		CuS, FeS, Ni_2S
	Platinum group minerals (PGM)		OsS_2, OsIrS
	Carbonates		Dol, Cal, Mgs
	Phosphates		Ap
	Oxide		TiO_2
Occurrence	Single phase		PGM, TiO_2, Ol, Di, Tr, Dol
	Multiphase	Two	Ol+Talc, Ol+Srp,Ol+Tr, Tr+Bt, Tr+Dol, Dol+Bt
		Three	En+Di+Ph, Tr+Ol+Ph, En+Ap+Bt, Ol+Ap+Bt, Dol+En+Ap, Dol+Tr+Bt, Tr+Di+Bt
		Four	En+Tr+Ap+Bt, Tr+Ap+BMM+Bt, Tr+Di+BMM+Bt, Tr+Ap+Dol+Bt, Tr+Di+Dol+Bt, Tr+Dol+Srp+Bt, Tr+Dol+BMM+Bt, Tr+Dol+BMM+Rt, Di+Dol+Cal+Bt

Table 1. Array of inclusions in chromite grains documented from the Zunhua chromitites using SEM-EDS. Abbreviations: Ap-Apatite; BMM-Base metal mineral; Bt-Biotite; Cal-Calcite; Di-Diopside; Dol-Dolomite; En-Enstatite; Ol-Olivine; PGM-Platinum group minerals; Ph-Phlogopite; Rt-Rutile; Srp-Serpentine; Talc-Talc; Tr-Tremolite.

4.2. Identification and Verification of TiO_2 (II)

There is a wide range of different inclusions preserved within the Zunhua chromitites as summarized in Table 1. We focused on a multi-phase inclusion composed of apatite, amphibole, rutile and a UHP polymorph of titanium dioxide (TiO_2 (II)) (Fig. 6). Results of our EDX semi-quantitative analyses are shown in Fig. 7. Table 2 shows a comparison of d-spacings measured from diffraction patterns of two HREM images and one SEAD image from this study with calculated data of TiO_2 (II) from literature (El Gorsey et al., 2001).

Table 2
Comparison of d-spacings measured from diffraction patterns of two HREM images and one SEAD image from this study with calculated data of TiO_2 (II) from literature (El Gorsey et al., 2001). a_0 = 4.535 Å, b_0 = 5.499 Å, c_0 = 4.900 Å

HREM obs (Å)		SAED obs (Å)	Mean obs(Å)	Calc (Å)	indexed planes of TiO_2 (II)
5.55	5.58	5.32	5.483	5.50	(010)
2.74	-	2.66	2.70	2.75	(020)
4.33	4.64	4.48	4.48	4.54	(100)
3.58	3.63	3.43	3.46	3.49	(110)
2.14	-	2.24	2.19	2.26	(200)

Note: Obs is short for observation; Calc is short for calculation.

To verify the structure of a crystal, it is necessary to further measure the lengths of diffracting vectors that represent the $1/d_{hkl}$ and angles between adjacent diffracting lattice planes. We measured the angles between planes from two different FFT diffraction patterns and compared them to calculated angles from known mineral phases. The diffraction patterns display the following set of angles between planes: the angle between (110)/(100) = 39.8° (39.47° calculated); the angle between (110)/(010) = 50.2° (50.53° calculated) (more data in Table 3). Based on the excellent match between observed and calculated data, the TiO_2 phase is confidently and unambiguously identified as TiO_2 (II) with an orthorhombic α-PbO_2structure, the ultra-high pressure (UHP) polymorph of rutile (TiO_2).

Table 3

Angles between lattice planes of the observed TiO_2 (II) from this study and calculated TiO_2 (II)from the literature (El Gorsey et al., 2001).

Planes	Calc (°)	HREM obs (°)	SAED obs (°)
(110) | (100)	39.47	40.50	39.80
(110) | (010)	50.52	52.80	50.20
(220) | (200)	39.47	38.75	
(220) | (020)	50.52	53.00	
(120) | (100)	58.74		59.30
(120) | (020)	31.26		30.90
(130) | (100)	67.96		68.10
(130) | (030)	22.04		21.70

4.3. Microstructural relationships of the multi-phase inclusion containing UHP TiO_2 (II)

We have identified the first Archean UHP inclusion in an orogenic podiform chromitite (section 4.2). The host chromite grain for the TiO_2 (II) is in a chromitite sample from the serpentinized dunite pod within harzburgite at the Zhuling location (Fig. 1 b,e).The host chromite grain is 250 μm in diameter and is surrounded by altered fibrous minerals including serpentine and talc (Fig. 3e,f). The multi-phase inclusion containing TiO_2 (II) is isolated, clearly separated from any cracks, and thus is interpreted to be a primary feature (Fig. 6a). There is no evidence for cracks in chromite even on a nanometer scale in the SEM images or in the TEM sample (Fig. 6). Therefore, the phases trapped inside the chromite pressure-vessel have been sealed and isolated since they formed in the Archean, until we cut them open, so they were shielded from fluids, and the pressure of the surrounding chromite grain did not allow decompression reactions to take place; it has been a closed system for > 2.5 billion years. Most regional metamorphic UHP rocks form in open systems, influenced by fluids and decompression of the host rocks (Wang et al., 2014; Xia et al., 2018), whereas we are presenting data from a closed system within the multi-phase inclusions encapsulated in the chromite. Our observations thus can be considered as a very rare occurrence of completely preserved inclusions in a host mineral.

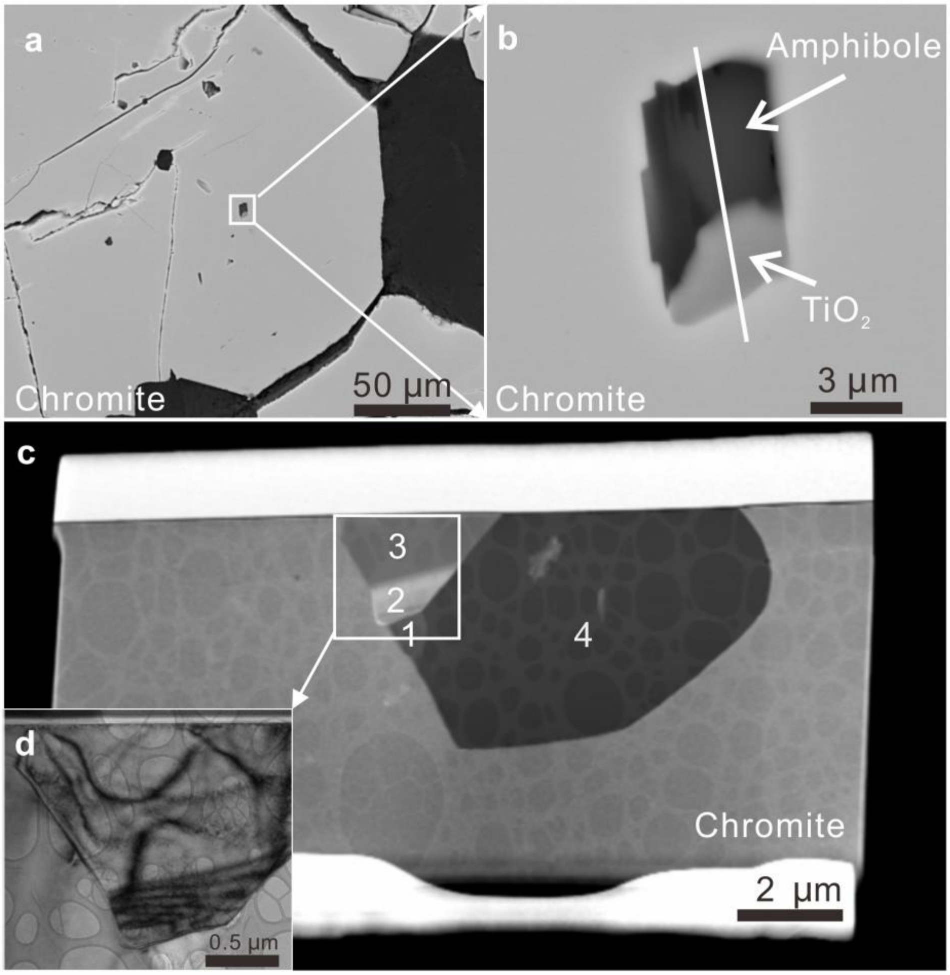

Fig. 6. Back-scattered electron (BSE) image from SEM, high-angle annular dark field (HAADF) Z-contrast image, and EDX data from TEM of a chromite grain with a multi-phase inclusion, from sample location shown in Fig. 1e and 1f. (a) BSE image shows part of the chromite grain containing the inclusion. (b) BSE image of the multi-phase inclusion within the chromite grain. The white line shows the FIB cutting position. (c) HAADF Z-contrast image shows a multi-phase inclusion in the chromite. Note the perforated carbon support film in the background (making the leopard-skin appearance) on which the TEM foil is resting; the bright material at the top is a platinum protection layer and the bright layer at the bottom is re-deposited sputtered material. Four areas in the inclusion are defined by different grey scale contrasts; (1) apatite, (2) TiO_2 (II), (3) rutile, (4) amphibole. Note that the contrast of the TiO_2

(II) grain is brighter than the rutile, because of its higher density. The apatite grain (1) is small and has a similar contrast to the adjacent amphibole.(d) Bright Field image of the selected area in (c). The rutile is characterized by curved dark diffraction contrast lines whereas the TiO_2 (II) polymorph shows 5 dark parallel diffraction contrast lines that are due to an inclined interface.

The multi-phase inclusion displays an irregular interface with chromite (Fig. 6b). Note the irregular shape of the interface between the inclusion and chromite has two rounded edges and an arrow-like appearance in the upper part. Overall, it is not the shape of a negative crystal in which the inclusions have nucleated and grown. The shape of the inclusion is affected by the size and arrangement of its component minerals, strongly suggesting an overgrowth of an existing mineral assemblage by chromite. The multi-phase inclusion (Fig. 6) is composed of TiO_2 and amphibole as determined by Energy Dispersive X-ray (EDX) analyses with SEM. After FIB cutting and preparation, apatite, amphibole, and two TiO_2 phases were identified using (EDX) analyses (Fig. 7).The EDX analysis on the apatite (F-rich) by TEM showsa composition of (in atomic percentage, simplified as in at. %): F = 7.71, P = 35.34, Ca = 56.93, and an analysis of amphibole by SEM shows a composition of (in atomic %): O = 68.90, Mg = 10.04, Si = 16.92, Ca=4.14. Rutile, F-apatite and amphibole are typical minerals in crustal rocks (F-apatite usually grows from silicate melt, not from magmatic-hydrothermal fluid) but TiO_2 (II) is a rare UHP phase found in both crustal and mantle rocks and meteorites (Dobrzhinetskaya et al., 2009; Hwang et al., 2000; Wu et al., 2005; Wirth et al., 2009; El Gorsey et al., 2009).

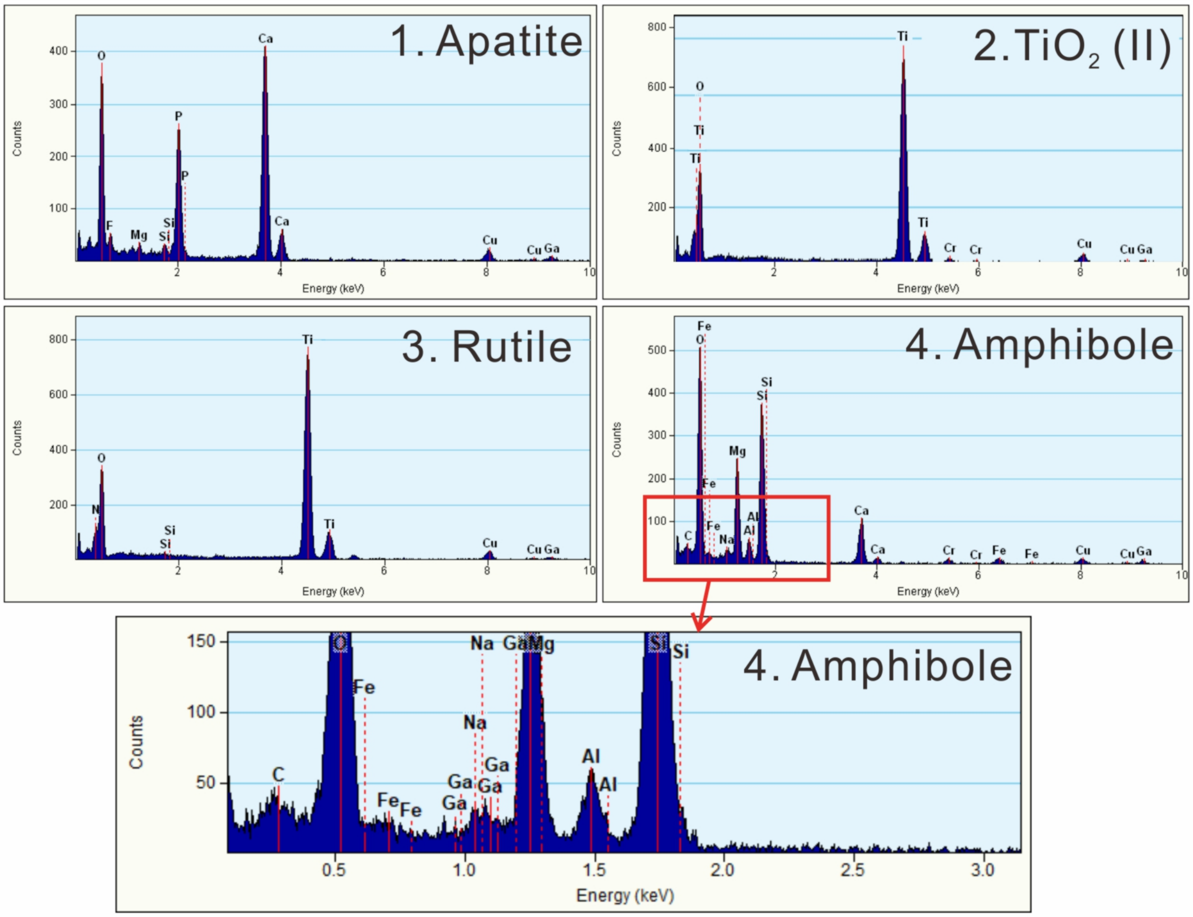

Fig.7. EDX analyses of the multi-phase inclusion. The analysis positions are shown in Fig. 3c.

4.4. Formation of UHP TiO_2 (II)

Although rare, TiO_2 (II) has been previously found in several Phanerozoic UHP orogenic settings, including as an inclusion in garnet of the Saxonian Erzgebirge diamondiferous quartzo-feldspathic rocks (Hacker and Gerya, 2013; Gilotti, 2013), in omphacite from coesite-bearing eclogite (Wu et al., 2005), as an inclusion in coesite within a diamond (Wirth et al., 2009), and associated with coesite within a podiform chromitite of the Luobusa ophiolite (Dobrzhinetskaya et al., 2009). It is also known from shock-induced metamorphic rocks in meteorite impacts (El Gorsey et al., 2001) and spherules in meteorite ejecta (Smith et al., 2016). However, we rule out the possibility of a meteoritic spherule origin based on the well-documented mantle origin of the

Zunhua podiform chromites (Li et al. 2002; Huang et al., 2004; Kusky et al., 2004, 2007, 2016, 2020; Polat et al., 2006; Wang et al., 2019;Ning et al., 2020), the lack of shock-induced minerals or microstructures in the samples, and the composition of the host chromite is totally different from that of meteoritic spherules, which are typically Fe-Ni alloys or silica formed by gas phase condensation of an impact-produced rock-vapor cloud (Johnson and Melosh, 2012), and which also lack volatile and hydrous phases such as amphibole and F-apatite that are present in the Zunhua samples.

Experimental constraints on the P-T conditions for the formation of TiO_2 (II) (Withers et al., 2003) are shown in Fig. 8, with the pressure of the transition from rutile to TiO_2 (II) increasing with increasing temperature. Based on the microstructures of the rutile, apatite and amphibole in SEM and TEM images (Fig. 6), these grains must have been overgrown by chromite during chromite crystallization. The encapsulating crystallization temperature was previously determined to be 1000-1200 °C (Li et al., 2002; Huang et al., 2004; Kusky et al., 2007) so we simply use the phase diagram (Withers et al., 2003) (Fig. 8) to estimate the pressure. This shows that the TiO_2-TiO_2 (II) phase transition in our samples should have happened at 7.5-9 GPa. Additional constraints on the pressure are obtained from phase relationships of the other phases in the inclusion.

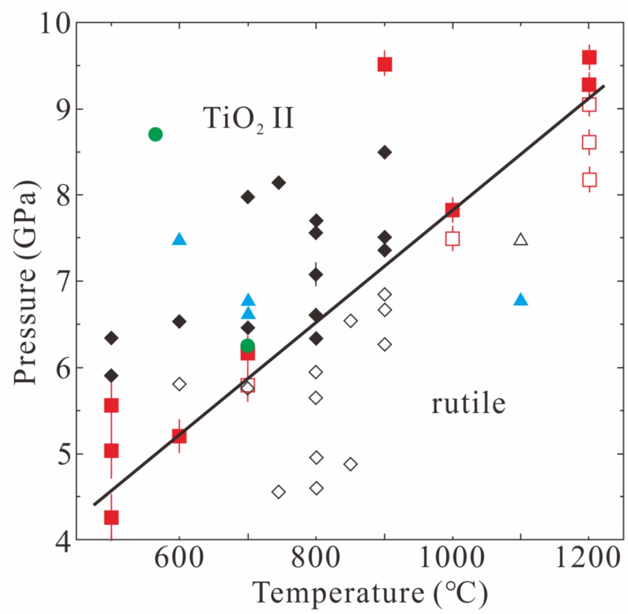

Fig. 8. Phase diagram for rutile-TiO_2 (II), modified from Withers et al. (2003). Filled symbols represent TiO_2 (II), and open symbols represent rutile. Squares are experimental results of Withers et al. (2003), diamonds are results of Akaogiet al. (1992), triangles are results of Olsen et al. (1999), and circles are results of Tang and Endo (1994).

4.5. Preservation and stability of UHP TiO_2 (II)

From the SEM and TEM images, we further note that there are no deformation features or dislocations in any of the phases, and the shape of rutile continues into the $\alpha-PbO_2$ structure meaning that it was a single UHP crystal at the time of incorporation into the host chromite. Furthermore, from the two diffraction patterns of the rutile and $\alpha-PbO_2$ we obtain the lattice plane spacing or hkl d-spacing (d_{hkl}) and from that we determine which lattice planes are parallel to each other yielding an orientation relationship of the lattice planes of the two phases:

$$(100)_{Ru} = 4.5937\ (A)\ //\ (100)_{\alpha-PbO2} = 4.535\ (A)$$
$$(021)_{Ru} = 1.8147\ (A)\ //\ (030)_{\alpha-PbO2} = 1.8330\ (A)$$
$$(121)_{Ru} = 1.6877\ (A)\ //\ (130)_{\alpha-PbO2} = 1.6978\ (A)$$

From these data it is obvious that the respective lattice plane spacings d_{hkl} are very similar, showing that this particular orientation is energetically favorable. Additionally, we can determine parallel directions in the two crystals; for example, direction[0-12] in rutile is parallel to [001] in α-PbO_2. Presenting the direction and the lattice planes fully describes the orientation relationship of rutile and α-PbO_2:

$$(100)_{Ru}//\ (100)_{\alpha\text{-}PbO2}$$
$$(021)_{Ru}//\ (030)_{\alpha\text{-}PbO2}$$
$$(121)_{Ru}//\ (130)_{\alpha\text{-}PbO2}$$
$$[0\text{-}12]_{Ru}//\ [001]_{\alpha\text{-}PbO2}$$

Thus, the rutile and α-PbO_2 exhibit a good match of lattice planes. The phase transition rutile – TiO_2 in the α-PbO_2 structure is a reconstructive phase transition, which is energetically facilitated by good matching lattices, as discussed below.

Chromite must have crystallized at ~1000–1250 °C, but temperatures above 1,200°C are not compatible with the presence of apatite. Apatite would have converted to tuite (γ -$Ca_3(PO_4)_2$,), the high-pressure form of apatite) at 1200 °C based on experimental data on samples with a starting composition of MORB (Konzett and Frost, 2009). With experimental compositions of basalt and Mg-basalt (similar to that of the multi-phase inclusion), hydroxyl apatite was shown to be unstable above 7.5 GPa at 950°C (Konzett and Frost, 2009) (*In our case it is F-apatite, for which there are no experimental constraints, so we assume that it is similar to hydroxyl apatite).* Because what we observe is structurally apatite, not tuite, in the inclusion, with no deformation features or signs of a phase transformation from tuite to apatite, this provides an additional constraint on our previous temperature estimate of 1000–1250°C, putting us at the lower limit because of the presence of apatite. This temperature is also in good agreement with the PT stability of rutile and rutile in α-PbO_2 (Withers et al., 2003) structure (TiO_2 (II)). We should observe apatite + rutile and/or α-PbO_2, in the inclusion at P-T conditions of 7.5GPa and 1000°C (Konzett and Frost, 2009), which is in agreement with the phases present, and the temperature range estimated for the crystallization of the chromite around the inclusions. The amphibole (tremolite) is stable through the PT conditions mentioned, until it breaks down at 1000–1100°C (Chernosky et al., 1998).

We therefore have excellent constraints for a temperature of approximately 1000°C to explain the presence of apatite and tremolite in the inclusions. That temperature yields a pressure of 7.5 GPa from both phase diagrams. These P-T conditions also explain why tremolite is still stable and did not transform into diopside +enstatite+quartz +water (Chernosky et al., 1998), providing yet an additional constraint for the P-T conditions being 7.5GPa and 1000°C.

Due to slow cooling from high temperature during exhumation we can assume a long thermal treatment (annealing) that removed any defects from the crystals. Accepting that TiO_2 – apatite and amphibole were overgrown by chromite at a pressure of 7.5–9 GPa (depth 270–330 km) then TiO_2 was structurally α-PbO_2 (chemically TiO_2 (II)). Thus, what we observe today in the multi-phase inclusion is a partial back-transformation of α-PbO_2 into the rutile structure. That reconstructive phase transformation nucleated at the apatite/TiO_2 (II) phase boundary growing into the TiO_2 (II) phase. Back-transformation was stopped due to the volume increase during the back-transformation thus generating a pressure increase within the inclusion during uplift.

5. Discussion

5.1. Deep subduction and recycling of crustal minerals in the Archean

There are few direct ways to study Earth's deep interior, thus most inferences about the character of the deep mantle are based on studies of geophysics, meteorites, and high-pressure experiments. Only in rare cases can small samples such as high-pressure polymorphs of olivine (ringwoodite) or $CaSiO_3$ perovskite be brought from the deep mantle to the surface in kimberlitic diamonds (e.g.,Nestola et al., 2018) or by mantle convection to be incorporated in podiform chromitites of ophiolites (Dobrzhinetskaya et al., 2009; Zhou et al., 2014; González-Jiménez et al., 2017; Lian et al., 2020). Such minerals offer a rare direct way to investigate Earth's deep interior. Cubic chromite is an ideal micro-container of relict UHP mineral phases because it is mechanically strong, highly refractory, isotropic in thermal contraction and stable over a wide range of P-T conditions (Dobrzhinetskaya et al., 2009; Yang et al., 2014).

Based on our microscopic, SEM, TEM, and Raman observations of the Zunhua samples, and their geological relationships, including thermal expansion coefficients and the bulk moduli of the concerned phases (supplementary data file S2), we propose the following hypothesis (Fig. 9) for the formation and preservation of the inclusion and its UHP phase. Crustal material, including rutile, apatite, and amphibole (as well as the carbonates and other minerals in other inclusions) were part of a subducting oceanic slab that reached a depth of at least 270 km between 2.6 and 2.55 billion years ago (path a-b-c on Fig. 9a). At this stage the rutile converted to TiO_2 (II) (with an α-PbO_2 structure) at approx. 7.5 GPa, but apatite and tremolite and chromite were still stable.

The crustal minerals (tremolite, apatite and UHP rutile or TiO_2 II) were separated from the subducting slab and entrained in the circulating mantle as the slab rolled-back or in early stages of subduction, which both disrupt the normal flow of the mantle, inducing upward flow above the slab (Kusky et al., 2014; Stern and Gerya, 2018) (path c-d on Figs. 9a, 9b). The exact process of transferring material from the lower plate to the overriding mantle wedge may have involved serpentinite diapirism of material from the subduction channel, intruding into the upper plate, as recently documented from American Samoa (Jackson et al., 2007), in the Calabrian arc (Polonia et al., 2017),at Gaussberg, Antarctica (Murphy et al., 2002), and invoked as a general process that may even help explain the diversity of arc magmatism (Codillio et al., 2018; Cruz-Aribe et al., 2018; Nielsen and Marschall, 2017). Zhang et al. (2019) show experimentally that partial melting of mixed sedimentary/peridotite material from the subduction channel at conditions (~300 km) similar to ours (4-15 GPa, 1200-1800 C) is possible, producing melts with both melted peridotite characteristics and traces of the sedimentary material. We suggest the xenocrystic inclusions represent un-melted remnants of this material transferred from the subduction channel to the overriding mantle wedge. We estimate from the make-up of the multi-phase inclusion that it was originally a very small (unrepresentative) piece of mafic material from the slab that was entrained in the subduction channel and transferred to the overriding mantle wedge during subduction (path b-c-d on Figs. 8a, 8b). This was just one inclusion, probably transferred together with the other inclusions (Table 1) in a serpentinite-mélange diapir, characteristic of rocks we have mapped (Fig. 1) in the Zunhua mélange. The process is similar to that recently documented for serpentinite diapirs above subducting slabs that are shown to transfer material from the subducting to the overriding plate (Polinia et al., 2017), perhaps eventually forming schlieren in the harzburgite (Fig. 1f and Fig.8b, location d).

Numerical models (Stern and Gerya, 2018) show that slab material can be brought up to near the surface from > 200 km through the change in mantle circulation in the mantle wedge overlying the subducting plate during subduction initiation or slab rollback, and incorporated into fore-arc spreading systems. In models of Stern and Gerya (2018) both solid and molten parts of subducting oceanic lithosphere can be incorporated into the overlying rising mantle wedge, and the zone of melt generation in the mantle wedge above the slab extends below 200 km depth. Adiabatic upwelling of mantle to accommodate space created by slab rollback (Kusky et al.,

2014) (Fig. 9b) generates high-Mg melts, forming highly mafic dikes (likely boninitic as shown by Ning et al., 2020, and Huang et al. 2021), reacting with harzburgite to form remnant dunite + chromite pods that cut the harzburgite host with trapped xenocrysts from the mantle harzburgite, and crustal minerals derived from schlieren scraped off the down-going slab (location d on Fig. 9b), at 7.5 GPa (270 km) and 1000°C. Thus, in addition to trapping crustal minerals such as the apatite, tremolite, rutile (TiO_2) and carbonates (Table 1), small xenocrysts of ambient mantle were trapped as inclusions, including olivine, orthopyroxene (from a harzburgite host), sulfides, base metals and native elements (PGM) (Table 1) that may have come from deep mantle sources (c.f., Yang et al., 2014). The presence of F-apatite also implies that apatite, TiO_2 and amphibole were trapped at depths > 200 km, because F-apatite typically grows from a silicate melt whereas OH-apatite grows from magmatic hydrothermal fluids (Li and Costa, 2020).

Fig.9. Tectonic model for the formation and preservation of the UHP TiO_2 II inclusion in the ophiolitic podiform chromite mélange (vertical scale condensed). In panel (a), crustal material from the passive margin sequence and from the accretionary prism is subducted to at least 270 km, where the rutile converts to the UHP phase TiO_2 II (path a-b-c). Flow in the mantle wedge parallels the subduction. Panel (b) shows slab rollback inducing a change in mantle flow to accommodate space created by slab rollback (Kusky et al., 2014) such that some of the deeply subducted material (plus xenocrysts of the ambient mantle, likely transferred to the upper plate in serpentinite diapirs (Polonia et al., 2017)) including the UHP-inclusion bearing chromites are encapsulated in the highly-mafic dikes and dunite pods. These are then entrained in upward flow (location d), and incorporated into the oceanic lithosphere (location e) at the crust/mantle interface in a fore arc spreading center (path c-d-e). Sketch in (b) for location d is based on outcrop data (Fig. 1e) from the field area, and for location e is based on thin section in Fig. 3d. (c) Collision of the arc terrane with the continent (EB - East Block of the North China Craton) at 2.5 Ga emplaces the ophiolitic mélange that preserves the UHP inclusions in the podiform chromite blocks (position f), with accompanying late deformation and metamorphism. Block diagram is sketch of thin section and surface of FIB foil through the inclusion with UHP TiO_2 (II).

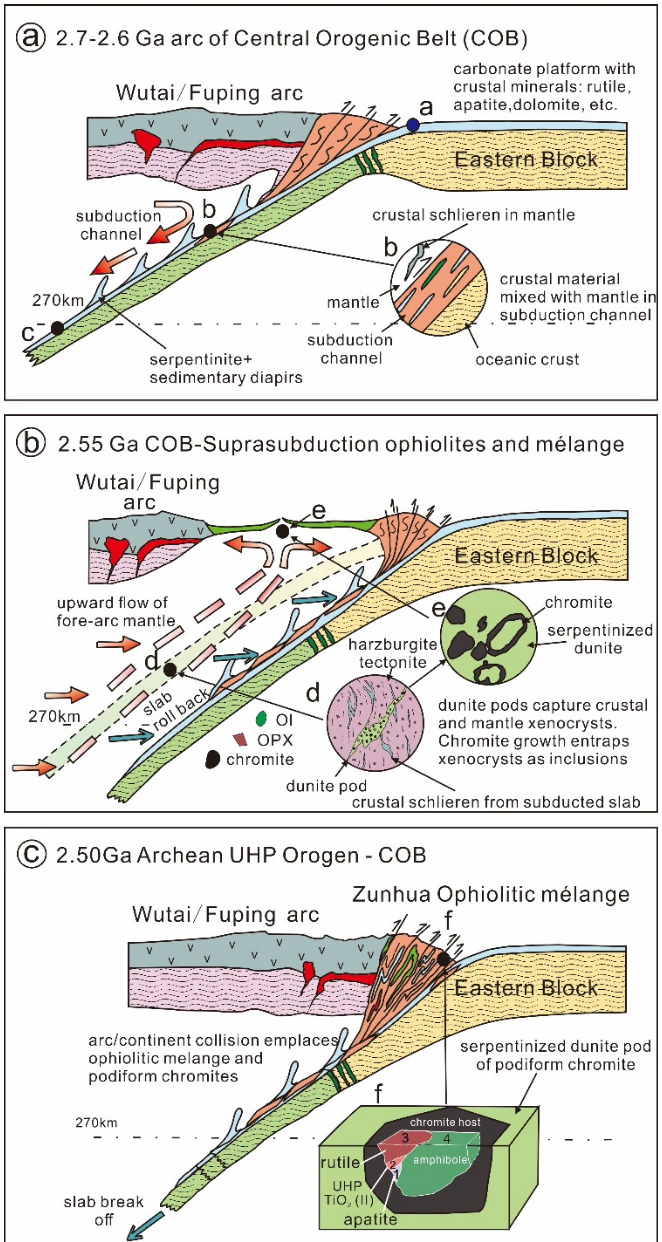

Numerical simulations of subduction processes (Stern and Gerya, 2018) show that soon after subduction initiation mantle flow is upward above the subducting slab (as in Fig. 9b), with temperatures above 1000°C, and a thin zone of melt brings mantle harzburgite with melts up into the fore-arc region to generate fore-arc ophiolites. In companion papers (Ning et al., 2020; Huang et al., 2021), we present evidence that the chromites from Zunhua interacted with a Mg-rich melt with boninitic affinity, which is considered characteristic of subduction initiation in forearc zones (Stern and Gerya, 2018; Rollinson, 2019).The mantle wedge at this stage is contaminated with serpentinite diapirs derived from the lower plate (Polinia et al., 2017), “schlieren,” and various small pieces of the subducted slab (location and sketch d in Fig. 9b), are incorporated into the magmas generated by partially melting the harzburgite (Fig. 9b). As the chromite grows within these highly mafic dikes and dunite pods it encapsulates the inclusions, at 1000°C and 7.5 GPa. This is witnessed by the shape of the inclusion presented in Fig. 6b. Upwelling in the mantle circulates this segment of deep mantle upward to become the mantle section beneath a forearc spreading center at 2.55 Ga. At this stage our samples would have been transported from > 270 km to < 10 km depth, where they became part of the fore-arc oceanic crust of an intra-oceanic arc system(position e on Fig. 9b), that collided with the Eastern Block of the NCC (Fig. 9c), deforming the fore-arc ophiolite and forming the Zunhua mélange (position f on Fig. 9c), preserved in the upper plate of accretionary orogen on the surface today (Kusky et al., 2018; Wang et al., 2019; Ning et al., 2020).

During its rise to the surface the UHP TiO_2 (II) was preserved because it was sealed inside the impervious chromite pressure vessel (Fig. 9c). Thermal expansion of all phases, especially tremolite, allowed the UHP phase to stay at UHP conditions since entrapment. The extra pressure exerted by the expanding tremolite was greater than that of the smaller expansion of the host chromite. This was countered by the opposite effect of the bulk moduli, as the external pressure decreased during exhumation (supplementary file S1).The thermal contraction of rutile and apatite and amphibole is 2X larger than that of chromite (supplementary Table 1). Consequently, rutile, apatite and amphibole shrink faster than chromite as the rock cools after crystallization, suggesting that no deformation will occur within the inclusions. If there had been defects in the rutile, apatite, and amphibole, they would have been healed by annealing during uplift thus moving the defects to the crystal surfaces or inclusion/host interfaces. However, there are no signs of damage or deformation in the rutile, apatite and amphibole. The above is consistent with all the phase relationships, mineral physics, microfabrics, and geological relationships. The combined field and P-T data on the inclusions provide unique constraints on the depth of subduction of both continental and oceanic material in the late Archean. In younger orogens, such as Sulu, the presence of intragranular coesite and inclusions in microdiamonds suggests subduction of continental material to at least 150 km (Wang et al., 2014; Xia et al., 2018). In the case of Zunhua, inclusion of continental crustal material in the podiform chromitites is more complex, but indicates subduction to at least 270 km. The return flow was different from that in classical blueschist/eclogite terranes (Hacker et al., 2013), but may be applicable to understanding emplacement of UHP ophiolitic mélanges and chromitites in many Phanerozoic and Precambrian orogens (Yang et al., 2014; Kusky et al., 2018, 2020).

There is still considerable controversy over the tectonic/dynamic processes that bring UHP inclusions in ophiolitic podiform chromitites to the surface in Phanerozoic ophiolites, but diamonds and suites of UHP and highly-reduced inclusions, very similar to those in the Zunhua podiform chromitites have now been identified in many ophiolites world-wide (Dobrzhinetskaya et al., 2009; Yang et al., 2007, 2014; Lian et al., 2020). The model we propose here may be generally applicable to podiform chromites containing UHP inclusions of all ages throughout the world. Although our findings open many questions about the relationships between deep mantle dynamics, the deep carbon cycle, and lithospheric tectonics, our documentation of circa > 2.55 Ga UHP inclusions in a 2.55 Ga ophiolitic podiform chromitite, along with a suite of inclusions similar to those in Phanerozoic podiform chromitites, shows clearly that the tectonic/dynamic processes that bring these deep mantle minerals back to the surface today, have been operating for at least the last 2.5–2.6 Ga, if not longer. Our results show that the structural and thermal conditions in Archean subduction zones and accretionary orogens were similar to those of the Phanerozoic.

5.2.Deeper implications for Archean tectonics.

Our results document that the Central (Taihang) Orogenic Belt of the North China Craton is the world's first recognized UHP Archean orogen. The Central Orogenic Belt is also the world's first well-constrained spatially and temporally linked Archean paired metamorphic belt (Huang et al, 2020), preserving contemporaneous parallel belts of high dT/dP (720-1200 °C/GPa) and intermediate dT/dP 425-600 °C/GPa) which is considered diagnostic of the asymmetric thermal structure of Phanerozoic subduction systems (Brown et al., 2020), showing that the Central Orogenic Belt of the NCC is the world's first-recognized Archean UHP paired metamorphic accretionary orogen. Together, this is the strongest evidence yet for the operation of asymmetric subduction to depths approaching the mantle transition zone, showing similar depth scales of Phanerozoic and Archean orogens.

The length scales of subduction in the Central (Taihang) Orogenic Beltare on a scale of thousands of kilometers (the orogen, or paleo-subduction zone, is 1600 km long) much like that on present-day Earth. The time scales of the early subduction have been constrained in our related work to have been at least 2.6–2.55 Ga; Ning et al., 2020), or 2.68-2.52 Ga (Kusky et al., 2020). This was followed by fore-arc extension and arc evolution (2.55-2.52 Ga; Ning et al., 2020; Deng et al., 2018), to collision, well constrained by the ages of metamorphic minerals in syn-collisional fabrics, and cross-cutting undeformed igneous dikes (2.50 Ga; Wang et al., 2019; Xiao et al., 2021). Late stages of the end-Archean orogeny were marked by uplift and erosion of the orogen to produce a foreland basin (2.48 Ga; Huang et al., 2019) with associated high-grade metamorphism in the hinterland (2.48 Ga; Kusky et al., 2016), and arc-polarity reversal (2.50-2.48 Ga; Kusky et al., 2016;Deng et al., 2018). The time scales of these events in the Central (Taihang) Orogenic Belt are all remarkably similar to the time scales of contemporary (i.e., Banda arc/Australia collision) and Phanerozoic examples of arc continent collisions (Pliocene of Taiwan; Cretaceous for the Caribbean arc; Oligocene in the Appinides; Miocene across the Philippines; and Ordovician up in the Grampian), typically lasting only a few to tens of millions of years (Brown et al., 2011). Thus, we have shown that the length, depth, and time scales of late Archean convergent margin processes were all indistinguishable from those of the Earth in the past 500 million years.

Because of the higher heat production in the Archean (Korenaga, 2013; Herzberg et al., 2010) there has been much modeling and speculation that mantle temperatures may have been significantly higher, thus preventing subduction (c.f.van Hunen and Moyen, 2012), or may have been significantly different from the modern style of subduction (c.f. Zheng and Zhao, 2020; Kusky, 2020). However, Aulbach and Arndt (2019) have argued that mantle temperatures have not exceeded present values by more than 100°C over the past 3.0 Ga, and Agrusta et al. (2018)

use numerical modeling to suggest that warmer mantle temperatures set up conditions that enhanced deep subduction and facilitated recycling of volatiles to the deep mantle.

Another line of argument against modern-style plate tectonics in the Archean is based on the now-disproven lack of documentation of UHP phases in Archean orogens, lack of documented spatially and temporally linked paired metamorphic belts, and lack of ophiolites and mélanges in the Archean record (e.g., Stern, 2008). In this work we document that all such features are present in the Central (Taihang) Orogenic Belt of the NCC. In other works, we have documented Archean ophiolitic fragments (ophirags), and ophiolitic mélanges, showing clear evidence of seafloor alteration, throughout the 1600 km long COB (summarized in Kusky, 2004; Kusky et al., 2020; Jiang et al., 2020). With the clear documentation now of all of the above key tectonic indicators for convergent margins and deep subduction in the Archean, we argue with confidence plate tectonics has been operating at least since the late Archean, and possibly longer (e.g., Kusky et al., 2018; Windley et al., 2021).

It has been argued that plate tectonics can not be proven to have operated on Earth until it can be proven that there was an established globally linked network of weak plate boundaries (Lenardic, 2018; Brown et al., 2020). However, as pointed out by Windley et al. (2021) and Kusky et al. (2021) this is a non-testable proposition, since the size of the preserved Archean regions (generally cratons or fragments within them) is remarkably small, with many regions (such as Isua, or Nulliak, or Nuvaguttiuk) only tens of km in area, and others such as the eastern Pilbara only measuring 200 x 200 km. The Central (Taihang) Orogenic Belt is 1600 km long, making it one of the largest well-studied Archean orogens, and having established geological signatures of subduction along the length of this orogen for tens to hundreds of Ma, to depths exceeding 270 km is more than a "local" effect. Through comparative tectonic analysis using the geologic indicators of plate interactions, we suggest that the Central (Taihang) orogen is but one of many preserved plate boundaries from the late Archean, with others in the Superior Province (Percival et al., 2012; Kusky and Hudleston, 1999), Yilgarn (Kusky et al., 2018), and most other cratons, as summarized in Windley et al. (2021).

6. Conclusions

The presence of both crustal and mantle mineral phases in an Archaean orogenic ophiolitic podiform chromite mélange demonstrates that deep subduction of shallow crustal materials and return flow took place in the Neoarchean. Our discovery of the UHP phase, TiO_2 (II), provides direct physical evidence for plate tectonics in the Archean and direct mineralogical evidence for deep subduction on early Earth. The Central (Taihang) Orogenic Belt of the North China Craton is the world's first-recognized ultra-high pressure (UHP) paired metamorphic orogen.

Author Contributions

The project was conceptualized by T.K.,designed by T.K., L.W., R.W., P.T.R., and A.P., and was administered by T.K. and L.W. Funding was obtained by T.K., L.W., Y.H., A.P., and P.T.R.. Field work was conducted by T.K., W.L., W.B.N., A.P., Y.H. and Y.Z. Analytical results were obtained by Y.H., R.W., L.W, and P.T.R.. Assessment of data, construction of models and regional results, writing and drafting were done by all authors.

Declaration of Competing Interests

The authors declare no competing financial or other interests.

Data Availability

All data used in this manuscript are included in the text, Supplementary Data, or in the cited published manuscripts.

Acknowledgements

We thank Anja Schreiber for preparing the electron transparent FIB foils. This work was supported by the National Natural Science Foundation of China (Nos. 41672212, 41572203, 91755213, 41902036), the MOST Special Fund and the Opening Fund of State Key Laboratory of Geological Processes and Mineral Resources, China University of Geosciences (Wuhan) (MSFGPMR02-3, GPMR201607), the Postdoctoral Science Foundation of China (No. 20100471203) and a research grant by Natural Sciences and Engineering Research Council (Canada). We thank Victoria Pease for efficient editorial handling of the paper, and two anonymous reviewers for their helpful comments.

References

Agrusta, R., van Hunen, J., and Goes, S., 2018. Strong plates enhance mantle mixing in early Earth, Nature Communications.doi.org/10.1038/s41467-018-05194-5

Akaogi, M., Kusaba, K., Susaki, J.-I., Yagi, T., Matsui, M., Kikegawa, T., Yusa, H., Ito, E., 1992. High-Pressure High-Temperature Stability of αPbO$_2$-Type TiO$_2$ and MgSiO$_3$ Majorite: Calorimetric and in Situ X-Ray Diffraction Studies, pp. 447-455. doi.org/10.1029/GM067p0447

Arai, S., Ahmed, A.H., 2017. Secular change of chromite concentration processes from the Archean to the Phanerozoic, in: Mondal, S.K., Griffin, W.L. (Eds.). Elsevier, pp. 139-157.doi.org/10.1016/B978-0-12-811159-8.00006-8

Aulbach, S., Arndt, N.T., 2019. Eclogites as palaeodynamic archives: Evidence for warm (not hot) and depleted (but heterogeneous) Archaean ambient mantle. Earth and Planetary Science Letters 505, 162-172.doi.org/10.1016/j.epsl.2018.10.025

Brown, D., Ryan, P.D., Afonso, J.C., Boutelier, D., Berg, J.P., Calvert, A., Cook, F., DeBari, S., Dewey, J.F., Gerya, T., Harris, R., Herrington, R., Konstantinovskaya, E., Reston, T., and Zagorevski, A., 2011. Arc-Continent collision: The making of an orogen. In: D. Brown and P.D. Ryan (Ed.), Arc-Continent Collision, Frontiers in Earth Sciences, Springer-Verlag Berlin Heidelberg, pp. 477-493. doi.org/10.1007/978-3-540-88558-0_7

Brown, M., Johnson, T., 2019. Metamorphism and the evolution of subduction on Earth. American Mineralogist 104, 1065-1082. doi.org/10.2138/am-2019-6956

Brown, M., Johnson, T., Gardiner, N.J., 2020. Plate Tectonics and the Archean Earth. Annual Review of Earth and Planetary Sciences 48, 291-320. doi.org/10.1146/annurev-earth-081619-052705

Cawood, P.A., Hawkesworth, C.J., Pisarevsky, S.A., Dhuime, B., Capitanio, F.A., Nebel, O., 2018. Geological archive of the onset of plate tectonics. Phil. Trans. R. Soc. A 376(2132), 20170405.doi.org/10.1098/rsta.2017.0405

Chernosky, J.V., Berman, R.G., and Jenkins, D.M., 1998. The stability of tremolite: New experimental data and a thermodynamic assessment. American Mineralogist 83, 726-738. doi.org/10.2138/am-1998-7-805

Codillo, E.A., Le Roux, V.,Marschall, H.R. 2018. Arc-like magmas generated by mélange-peridotite interaction in the mantle wedge. NatureCommununications 9, 2864. https://doi.org/10.1038/s41467-018-05313-2

Cruz-Aribe, A., Marschall, H.R., Gaetani, G.A., Le Roux, V., 2018. Generation of alkaline magmas in subduction zones by partial melting of mélange diapirs- an experimental study, Geology 46, 343–346. https://doi.org/10.1130/G39956.1

Deng, H., Kusky, T.M.,Polat, A., Lan, B.Y., Huang, B., Peng, H.T., Wang, J.P., Wang, S.J., 2018. Magmatic record of Neoarchean arc-polarity reversal from the Dengfeng segment of the Central Orogenic Belt, North China Craton. Precambrian Research 326, 105-123.doi.org/10.1016/j.precamres.2018.01.020

Dobrzhinetskaya, L.F., Wirth, R., Yang, J., Hutcheon, I.D., Weber, P.K., Green, H.W., 2009. High-pressure highly reduced nitrides and oxides from chromitite of a Tibetan ophiolite. Proceedings of the National Academy of Sciences of the United States of America 106, 19233-19238. doi.org/10.1073/pnas.0905514106

El Goresy, A., Chen, M., Gillet, P., Dubrovinsky, L., Graup, G., Ahuja, R., 2001. A natural shock-induced dense polymorph of rutile with α-PbO_2 structure in the suevite from the Ries crater in Germany. Earth and Planetary Science Letters 192, 485-495.doi.org/10.1016/S0012-821X(01)00480-0

Festa, A., Ogata, A., Pini, A., 2019. Mélanges: 100th anniversary of the inception of the term and concept. Gondwana Research 74, 1-270.doi.org/10.1016/j.gr.2019.07.002

Gilotti, J.A., 2013. The realm of ultrahigh-pressure metamorphism. Elements 9, 255-260. doi .org/10.2113/gselements.9.4.255

Gonzalez, J.P., Baldwin, S.L., Thomas, J., Nachlas, W.O., and Fitzgerald, P., 2020, Evidence for ultrahigh-pressure metamorphism discovered in the Appalachian orogen: Geology, v. 48. doi.org/10.1130/G47507.1

González-Jiménez, J.M., Camprubí, A., Colás, V., Griffin, W.L., Proenza, J.A., O'Reilly, S.Y., Centeno-García, E., García-Casco, A., Belousova, E., Talavera, C., Farré-de-Pablo, J., Satsukawa, T., 2017. The recycling of chromitites in ophiolites from southwestern North America. Lithos 294-295, 53-72.doi.org/10.1016/j.lithos.2017.09.020

Hacker, B.R., and Gerya, T., 2013. Paradigms, new and old, for ultra-high pressure tectonism, Tectonophysics 603, 79-88. doi.org/10.1016/j.tecto.2013.05.026

Hacker, B., Gerya, T., and Gilotti, J., 2013. Formation and Exhumation of ultra-high-pressure terranes, Elements. doi.org/0.2113/gselements.9.4.289

Harrison, T.M., 2009. The Hadean Crust: Evidence from >4 Ga Zircons. Annual Review of Earth and Planetary Sciences 37, 479-505. doi.org/10.1146/annurev.earth.031208.100151

Herzberg, C., Condie, K., Korenaga, J., 2010. Thermal history of the Earth and its petrological expression. Earth and Planetary Science Letters 292, 79–88.doi.org/10.1016/j.epsl.2010.01.022

Holtzman, B., 2000. Gauging stress from mantle chromitite pods in the Oman ophiolite. Geological Society of America Special Paper 349, pp. 149-158. doi.org/10.1130/0-8137-2349-3.149

Huang, B., Kusky, T.M., Johnson, T.E., Wilde, S.A., Wang, L., Polat, A., Fu, D., 2020. Paired metamorphism in the Neoarchean: A record of accretionary-to-collisional orogenesis in the North China Craton. Earth and Planetary Science Letters 543, 116355. doi.org/10.1016/j.epsl.2020.116355

Huang, B., Kusky, T.M., Wang, L., Polat, A., Fu, D., Windley, B.F., Deng, H., Wang, J.P., 2019. Structural relationships and kinematics of the NeoarcheanDengfeng forearc and accretionary complexes, southern North China Craton. Geological Society of America Bulletin 131, 966-996.doi.org/10.1130/B31938.1.

Huang, X.N., Li, J., Kusky, T.M., Chen, Z., 2004. Microstructures of the Zunhua 2.50 Ga Podiform Chromite, North China Craton and Implications for the Deformation and Rheology of the Archean Oceanic Lithospheric Mantle. Developments in Precambrian Geology 13, 321-337. doi.org/10.1016/S0166-2635(04)13010-7

Huang, Y., Wang, L., Robinson, P., Ning, W.B., Zhong, Y.T., Wang, J.P., Hu, W., Polat, A., and Kusky, T., 2021, Podiform chromitite genesis in an Archean juvenile forearc: the 2.55 Ga Zunhuachromitites, North China Craton, Lithos, 106194,https://doi.org/10.1016/j.lithos.2021.106194

Hwang, S.L., Shen, P., Chu, H.T., Yui, T.F., 2000. Nanometer-size αPbO_2-type TiO_2 in garnet: A thermobarometer for ultrahigh-pressure metamorphism. Science 288, 321-324. doi.org/10.1126/science.288.5464.321

Jackson, M. G., Hart, S. R., Koppers, A. A. P., Staudigel, H., Konter, J., Blusztajn, J., et al. 2007. The return of subducted continental crustin Samoan lavas. Nature, 448(7154), 684–687. https://doi.org/10.1038/nature06048

Jiang, K., Wang, J.P., Kusky, T.M., Polat, A., Deng, H., Wang, L., 2020, Neoarchean seafloor hydrothermal metamorphism of basalts in the Zanhuang ophiolitic mélange, North China craton, Precambrian Research, doi.org/10.1016/j.precamres.2020.105832

Johnson, B.C., Melosh, H.J., 2012. Formation of spherules in impact produced vapor plumes. Icarus 217, 416-430. doi.org/10.1016/j.icarus.2011.11.020

Konzett, J., Frost, D.J., 2009. The high P-T stability of hydroxyl-apatite in natural and simplified MORB - An experimental study to 15 GPa with implications for transport and storage of phosphorus and halogens in subduction zones. Journal of Petrology 50, 2043-2062. doi.org/10.1093/petrology/egp068

Korenaga, J., 2013. Initiation and evolution of plate tectonics on Earth: theories and observations. Annual Review of Earth and Planetary Sciences 41, 117–151.doi.org/10.1146/annurev-earth-050212-124208

Kusky, T.M., editor, 2004, Precambrian Ophiolites and Related Rocks, Developments in Precambrian Geology 13, Elsevier Publishers, ISBN# 0444509232, 748 pp.

Kusky, T., 2020. Plate tectonics in relation to mantle temperatures and metamorphic properties. Science China Earth Sciences 63, 634-642. doi.org/10.1007/s11430-020-9597-5

Kusky, T.M., and Hudleston, P.J., 1999, Growth and Demise of an Archean carbonate platform, Steep Rock Lake, Ontario Canada. Canadian Journal of Earth Sciences, volume 36, p. 1-20. https://doi.org/10.1139/e98-108

Kusky, T.M., Li, J.H., Glass, A., and Huang, H., A., 2004, Origin and Emplacement of Archean Ophiolites of the Central Orogenic Belt, North China Craton, Chapter 7, in Kusky, T.M., Precambrian Ophiolites and Related Rocks, Developments in Precambrian Geology 13, Elsevier, Amsterdam, pp. 223-274.doi.org/10.1016/S0166-2635(04)13007-7

Kusky, T.M., Polat, A., Windley, B.F., Burke, K.C., Dewey, J.F., Kidd, W.S.F., Maruyama, S., Wang, J.P., Deng, H., Wang, Z.S., Wang, C., Fu, D., Li, X.W., Peng, H.T., 2016. Insights into the tectonic evolution of the North China Craton through comparative tectonic analysis: A record of outward growth of Precambrian continents. Earth-Science Reviews 162, 387-432. doi.org/10.1016/j.earscirev.2016.09.002

Kusky, T.M., Wang, J.P., Wang, L., Huang, B., Ning, W.B., Dong, F., Peng, H.T., Deng, H., Polat, A., Zhong, Y.T., and Shi, G.Z., 2020. Mélanges through time: Life Cycle of the world's largest Archean mélange compared with Mesozoic and Paleozoic subduction-accretion-collision mélanges, Earth Science Reviews. in post-revision review, EARTH_2020_75_R1.

Kusky, T.M., Windley, B.F., Polat, A., 2018. Geological Evidence for the Operation of Plate Tectonics throughout the Archean: Records from Archean Paleo-Plate Boundaries. Journal of Earth Science 29, 1291-1303. doi.org/10.1029/tc003i004p00429

Kusky, T.M., Windley, B.F., Wang, L., Wang, Z., Li, X., Zhu, P., 2014. Flat slab subduction, trench suction, and craton destruction: Comparison of the North China, Wyoming, and Brazilian cratons. Tectonophysics 630, 208-221. doi:10.1016/j.tecto.2014.05.028

Kusky, T.M., Zhi, X., Li, J., Xia, Q., Raharimahefa, T., Huang, X., 2007. Chondritic osmium isotopic composition of Archean ophiolitic mantle, North China craton. Gondwana Research 12, 67-76. doi.org/10.1016./j.gr.2006.10.023

Lenardic, A., 2018. The diversity of tectonic modes and thoughts about transitions between them, Philosophical Transactions of the Royal Society A 376, 20170416. http://dx.doi.org/10.1098/rsta.2017.0416.

Li, J., Kusky, T.M., Huang, X.N., 2002. Archean podiform chromitites and mantle tectonites in ophiolitic mélange, North China craton: A record of early oceanic mantle processes. GSA Today 12, 4-11. doi.org/10.1130/1052-5173(2002)012<0004:APCAMT>2.0.CO;2

Li, W., Costa, F., 2020. A thermodynamic model for F-Cl-OH partitioning between silicate melts and apatite including non-ideal mixing with application to constraining melt volatile budgets. Geochimica et Cosmochimica Acta 269, 203-222. doi.org/10.1016/j.gca.2019.10.035

Lian, D., Yang, J.S., Dilek, Y., Wiedenbeck, M., Wu, W.,Rocholl, A., 2020. Precambrian Zirconsin Chromitites of the Cretaceous Aladag Ophiolite (Turkey) Indicate Deep Crustal Recycling in Oceanic Mantle,Precambrian Research. doi.org/10.1016/j.precamres.2020.105838

Murphy, D. T., Collerson, K. D., &Kamber, B. S. (2002). Lamproites from Gaussberg,Antarctica: Possible transition zone melts of Archaeansubducted sediments. Journal of Petrology, 43(6), 981–1001. https://doi.org/10.1093/petrology/43.6.981

National Academies of Sciences, E., Medicine, 2020. A Vision for NSF Earth Sciences 2020-2030. National Academies Press, Washington, D.C. doi.org/10.17226/25761

Nestola, F., Korolev, N., Kopylova, M., Rotiroti, N., Pearson, D.G., Pamato, M.G., Alvaro, M., Peruzzo, L., Gurney, J.J., Moore, A.E., Davidson, J., 2018. $CaSiO_3$ perovskite in diamond indicates the recycling of oceanic crust into the lower mantle. Nature 555, 237-241. doi.org/10.1038/nature25972

Nicolas, A., 1989. Structures of ophiolites and dynamics of oceanic lithosphere. Structures of ophiolites and dynamics of oceanic lithosphere, Petrology and Structural Geology v. 4, Kluwer, Dodrect. doi.org/10.1007/978-94-009-2374-4

Nicolas, A., Al Azri, H., 1991. Chromite-rich and chromite-poor ophiolites: the Oman case. in: Peters, Tj., Nicolas, A., and Coleman, R.G., eds., Ophiolite Genesis and Evolution of the Oceanic Lithosphere. Petrology and Structural Geology v. 5, 261-274. Springer, Dodrecht. doi.org/10.1007/978-94-011-3358-6_14

Nielsen, S.G., and Marschall, H.R., 2017. Geochemical evidence for mélange melting in global arcs, Science Advances, 2017;3: e1602402.

Ning, W., Kusky, T., Wang, J., Wang, L., Deng, H., Polat, A., Huang, B., Peng, H., Feng, P., 2020. From subduction initiation to arc–polarity reversal: Life cycle of an Archean subduction zone from the Zunhua ophiolitic mélange, North China Craton. Precambrian Research,PRECAM_2020_106_R1, in post-revision review.

Olsen, J.S., Gerward, L., Jiang, J.Z., 1999. On the rutile/α-PbO_2-type phase boundary of TiO_2. Journal of Physics and Chemistry of Solids 60, 229-233. doi.org/10.1016/S0022-3697(98)00274-1

Peng, H., Kusky, T.M., Deng, H., Wang, L., Wang, J.P., Huang, Y., Huang, B., Ning, W.B., 2020. Identification of the NeoarcheanJianping pyroxenite-mélange in the Central Orogenic Belt, North China Craton: A fore-arc accretional assemblage. Precambrian Research 336, 105495. doi.org/10.1016/j.precamres.2019.105495.

Percival, J.A., Skulski, T., Sanborn-Barrie, M., Stott, G.M., Leclair, A.D., Corkery, M.T., Boily, M., 2012. Geology and tectonic evolution of the Superior Province, Canada. In: Percival, J.A., Cook, F.A., Clowes, R.M. (Eds.), Tectonic Styles in Canada: The Lithoprobe Perspective. Geological Association of Canada Special Paper 49, 321–378.

Polat, A., 2012. Growth of Archean continental crust in oceanic island arcs. Geology 40, 383-384. doi.org/10.1130/focus042012.1

Polat, A., Herzberg, C., Münker, C., Rodgers, R., Kusky, T., Li, J., Fryer, B., Delaney, J., 2006. Geochemical and petrological evidence for a suprasubduction zone origin of Neoarchean (ca. 2.5 Ga) peridotites, central orogenic belt, North China craton. Bulletin of the Geological Society of America 118, 771-784. doi.org/10.1130/B25845.1

Polonia, A., Torellie, L., Gasperini, L., Cocchi, L., Muccini, F., Bonatti, E., Hensen, C., Schmidt, M., Romano, S., Artoni, A., Carlini, M., 2017. Lower plate serpentinite diapirism in the Calabrian arc subduction complex, Nature Communications 8, 2172(2017), https://doi.org/10.1038/s41467-017-02273-x

Raterron, P., Girard, J., Chen, J., 2012. Activities of olivine slip systems in the upper mantle. Physics of the Earth and Planetary Interiors 200-201, p. 105-112. doi.org/10.1016/j.pepi.2012.04.006

Robinson, P.T., Trumbull, R.B., Schmitt, A., Yang, J.S., Li, J.W., Zhou, M.F., Erzinger, J., Dare, S., Xiong, F., 2015. The origin and significance of crustal minerals in ophiolitic chromitites and peridotites. Gondwana Research 27, 486-506. doi.org/10.1016/j.gr.2014.06.003

Rollinson, H., 2019. Dunites in the mantle section of the Oman ophiolite – The boninite connection. Lithos 334-335, 1-7. doi.org/10.1016/j.lithos.2019.03.008

Smith, F.C., Glass, B.P., Simonson, B.M., Smith, J.P., Krull-Davatzes, A.E., Booksh, K.S., 2016. Shock-metamorphosed rutile grains containing the high-pressure polymorph TiO2-II in four Neoarchean spherule layers. Geology 44, 775-778. doi.org/10.1130/G38327.1

Stern R.J., 2008. Modern-style plate tectonics began in Neoproterozoic time: an alternative interpretation of Earth's tectonic history. Geological Society of America Special Paper 440, 265–80.doi.org/10.1130/2008.2440(13)

Stern, R.J., Gerya, T., 2018. Subduction initiation in nature and models: A review. Tectonophysics 746, 173-198. doi.org/10.1016/j.tecto.2017.10.014

Tang J., and Endo, S., 1994. X-ray study of the transitions among the rutile, a-PbO2 and baddeleyite phases of TiO2 at high pressure and high temperature. In: Schmidt, S.C., Shaner, J.W., Samara, G.A., and Ross, M., eds; High-pressure science and technology.American Institute of Physics Conference Proceedings 309, pp 367–370. doi.org/10.1063/1.46118

Thayer, T.P., 1964. Principal features and origin of podiform chro-mite deposits, and some observations on the Guleman-Soridag District, Turkey. Economic Geology 59, 1497-1524. doi.org/10.2113/gsecongeo.59.8.1497

van Hunen, J, Moyen, J.F., 2012. Archean subduction: fact of fiction?, Annual Reviews of Earth and Planetary Sciences 40, 195-219. doi.org/10.1146/annurev-earth-042711-105255

Wallis, D., Hansen, L.N., Tasaka, M., Kumamoto, K.M., Parsons, A.J., Lloyd, G.E., Kohlstedt, D.L., Wilkinson, A.J., 2019. The impact of water on slip system activity in olivine and the formation of bimodal crystallographic preferred orientations. Earth and Planetary Science Letters 508, 51-61. doi.org/10.1016/j.epsl.2018.12.007

Wang, J.P., Li, X., Ning, W.B, Kusky, T., Wang, L., Polat, A., Deng, H., 2019. Geology of a Neoarchean suture: Evidence from the Zunhua ophiolitic mélange of the Eastern Hebei Province, North China Craton. Bulletin of the Geological Society of America 131, 1943-1964. doi.org/10.1130/B35138.1

Wang, L., Kusky, T.M., Polat, A., Wang, S., Jiang, X., Zong, K., Wang, J., Deng, H., Fu, J., 2014. Partial melting of deeply subducted eclogite from the Sulu orogen in China. Nature Communications 5, 5604-5604. doi.org/10.1038/ncomms6604

Wang, L., Blaha, S., Kawazoe, T., Miyajima, N., Katsura, T., 2017. Identical activation volumes of dislocation mobility in the [100](010) and [001](010) slip systems in natural olivine. Geophysical Research Letters 44, 2687-2692. doi.org/10.1002/2017GL073070

Windley, B.F., Kusky, T.M., and Polat, A., 2021. Onset of plate tectonics by the early Archean. Precambrian Research 352. 105980. https://doi.org/10.1016/j.precamres.2020.105980.

Wirth, R., Kaminsky, F., Matsyuk, S., Schreiber, A., 2009. Unusual micro- and nano-inclusions in diamonds from the Juina Area, Brazil. Earth and Planetary Science Letters 286, 292-303. doi.org/10.1016/j.epsl.2009.06.043

Withers, A.C., Essene, E.J., Zhang, Y., 2003. Rutile/TiO_2II phase equilibria. Contributions to Mineralogy and Petrology 145, 199-204. doi.org/10.1007/s00410-003-0445-2

Wu, X., Meng, D., Han, Y., 2005. α-PbO_2-type nanophase of TiO_2 from coesite-bearing eclogite in the Dabie Mountains, China. American Mineralogist 90, 1458-1461. doi.org/10.2138/am.2006.2202

Xia, B., Brown, M., Wang, L., Wang, S.J., Piccoli, P., 2018. Phase equilibrium modeling of MT-UHP eclogite: A case study of coesite eclogite at Yangkou Bay, Sulu Belt, Eastern China. Journal of Petrology 59, 1253-1280. doi.org/10.1093/petrology/egy060

Xiao, Deng, Ning, Wenbin, Wang, Junpeng, T. Kusky, L. Wang, Hao Deng, Yating Zhong, Kang Jiang, 2021, Neoarchean to Paleoproterozoic tectonothermal evolution of the North China Craton: Constraints from geological mapping and Th-U-Pb geochronology of zircon, titanite, and monazite in Zanhuang massif. Precambrian Research 359, 106214. https://doi.org/10.1016/j.precamres.2021.106214

Yang, J.S., Dobrzhinetskaya, L., Bai, W.J., Fang, Q.S., Robinson, P.T., Zhang, J., Green, H.W., 2007. Diamond- and coesite-bearing chromitites from the Luobusa ophiolite, Tibet. Geology 35, 875-878. doi.org/10.1130/G23766A.1

Yang, J.S., Robinson, P.T., Dilek, Y., 2014. Diamonds in ophiolites. Elements 10, 127-130.doi.org/10.2113/gselements.10.2.127

Zhang, L., Zhai, M., Zhang, X., Xiang, P., Dai, Y., Wang, C., Pirajno, F., 2012. Formation age and tectonic setting of the Shirengou Neoarchean banded iron deposit in Eastern Hebei Province: Constraints from geochemistry and sims zircon u-pb dating. Precambrian Research 222-223, 325-338.doi.org/10.1016/j.precamres.2011.09.007

Zhang, Y., Wang, C., Zhu, L., Jin, Z.,Li, W. 2019. Partial melting of mixedsedimentperidotite mantle source andits implications. Journal of GeophysicalResearch: Solid Earth, 124, 6490–6503.https://doi.org/10.1029/2019JB017470

Zheng, Y.F., Zhao, G.C., 2020. Two styles of plate tectonics in Earth's history. Science Bulletin 65, 329-334. https://doi.org/10.1016/j.scib.2018.12.029Zhong, Y.T., Kusky, T.M., Wang, L., Polat, A., Peng, Y.Y., Luan, Z.K., Liu, X.Y., and Wang, C.H., Wang, J.P., Alpine-style subhorizontal juvenile forearc nappes thrust of continental margin, North China, demonstrate large horizontal plate motions, Nature Communications, in revision,ms no. NCOMMS-21-16884.

Zhou, M.F., Robinson, P.T., Malpas, J., Edwards, S.J., Qi, L., 2005. REE and PGE geochemical constraints on the formation of dunites in the Luobusa ophiolite, Southern Tibet. Journal of Petrology 46, 615-639. doi.org/10.1093/petrology/egh091

Zhou, M.F., Robinson, P.T., Su, B.X., Gao, J.F., Li, J.W., Yang, J.S., Malpas, J., 2014. Compositions of chromite, associated minerals, and parental magmas of podiform chromite deposits: The role of slab contamination of asthenospheric melts in suprasubduction zone environments. Gondwana Research 26, 262-283. doi.org/10.1016/j.gr.2013.12.011

Contents of Supplementary Text

1. Analytical methods

1.1. Scanning electron microscopy (CUGW)

Scanning electron microscopy (SEM) with secondary electron imaging and back-scattered electron modes was used to observe the morphology of chromite grains. The composition of selected targets was acquired by SEM with energy-dispersive X-ray spectroscopy (EDS). SEM analyses were carried out in the State Key Laboratory of Geological Processes and Mineral Resources, China University of Geosciences, Wuhan using a FEI Quanta 450 field emission SEM. Standard operating conditions for SEM imaging and EDS analyses were 10–20 kV accelerating voltage, working distance of 10–13 mm, and electron beam current of 1 nA. Thin section samples were coated with a few nanometre of carbon prior to analysis.

1.2. Mineral phase identification by TEM. 1. FIB Sample Preparation (GFZ)

Analysis by transmission electron microscopy (TEM) requires electron transparent samples, obtained by milling thin foils with a thickness less than 0.15 µm (Wirth, 2009). Typical electron transparent foils made by FIB have dimensions of 15×10×0.15 µm. The FIB instrument (FEI FIB 200 TEM) operated at the GeoForschungsZentrum (GFZ), Potsdam was used for sample preparation. This single beam instrument allows lift-out of samples as ex-situ lift out only, following the procedures of Wirth (2004, 2009). Selected samples and locations where the foils were obtained were first studied under a petrographic microscope and SEM. For preparation of the foils, a Ga-ion beam (30 keV acceleration voltage) was focused onto selected locations of thin section surfaces to sputter material from the chromite grains.

1.3. Mineral phase identification by TEM. 2. Transmission Electron Microscopy (GFZ)

TEM investigations were performed using a TECNAI F20 XTWIN TEM operated at 200 kV with a field emission gun (FEG) as the electron source at the GFZ in Potsdam, Germany. The

TEM is equipped with a GatanTridiem™ energy filter, an EDAX Genesis™ X-ray analyzer with an ultra-thin window, and a Fishione high-angle annular dark field detector. A Tridiem energy filter was used for acquisition of bright and dark field images as well as high-resolution images applying a 20-eV window to the zero-loss peak. EDX spectra were acquired using the TIA software package in the scanning transmission mode of the TEM. To minimize mass loss due to electron sputtering during data acquisition the electron beam was scanned within a preselected area. The acquisition time of EDX spectra was 60 s.

1.4. Mineral phase identification by TEM. 3. Mineral Phase Confirmation

In situ EDX analysis was carried out on thetarget inclusion sample as the first step to obtain its semi-quantitative chemical components. This reduces the possible range of the unknown phase into a few choices of minerals that have similar chemical components but different crystal structures (polymorphs). Then, electron diffraction patterns from mineral phases were recorded on image plates by selected area electron diffraction (SAED) from which the observed d_{hkl} lattice plane distances of the mineral phases were measured. One image typically contains several diffraction spots that can be assigned to different lattice planes in the crystal. From the diffraction spots (diffraction vectors), we calculated-spacings between the lattice planesand the angles between adjacent vectors. Based on the chemical composition measured with EDX we deduce the presence of a particular phase. If the observed d-spacing and angles between adjacent planes match the calculated d-spacings and angles from a known structure, an unambiguous identification of the phase is possible. Error of measurement angles is $< 0.5°$ in electron diffraction patterns. Based on measured different d_{hkl} values the unit cell parameters can be calculated.

S.2.Supplementary File 2.

2.Evaluation of the possible role of overpressure on the formation and preservation of the UHP phase

To test if volume and pressure changes were important for the inclusions during increasing P-T conditions (subduction) or decreasing conditions (exhumation), we used data from the thermal expansion/contraction tables (Ahrens, 1995) for our estimates of possible overpressure within the inclusion vessel. Using the textural phase relationships described above, and considering the bulk moduli and thermal expansion coefficients for the phases concerned (Supplementary Table 1), it is possible that the phase transition occurred at the lower end of our pressure window (7.5 GPa), rather than the high-end estimate of 9 GPa. This suggestion is based on experimental data for the transition of apatite to its UHP equivalent, known as tuite (Konzett and Frost, 2009). Because we do not observe any signs of a phase transformation in our apatite grain, the phase diagram of Konzett and Frost (2009) suggests that our **maximum** estimate of 9 GPa (330 km) at 1,200°C is still within the stability field of apatite. On the other hand, estimating the **minimum** P-T conditions possible for our sample, it appears that both apatite and TiO_2 (II) could be stable at a temperature of 1,000°C and a pressure of 7–8 GPa. However, we need to consider a possible internal overpressure in the inclusion, because the thermal expansion coefficients (a_o (10^{-6}))of the phases in the inclusion are larger than that of the confining chromite grain (Supplementary Table 1). Thus, if the crustal minerals that form the inclusion were trapped by a chromite grain growing from a highly mafic (boninitic) melt at 7–8 GPa (as shown by the textural relationships described above), their temperature would suddenly rise from that of the cooler ambient slab that brought them to the appropriate depth, but would then cool slowly as they rose to the surface. Because the inclusions have a larger thermal expansion coefficient than the host chromite (Supplementary Table 1), they may have originally expanded slightly, thus increasing internal pressure. Thus, it may not have been necessary to subduct the sample as far as our maximum pressure boundary (9 GPa or 330–430 km) to initiate the transition of rutile to TiO_2 (II). For example, such an overpressure may allow the sample to achieve an internal pressure >7.5 GPa at depths as shallow as 270 km.So, in total our observations are in accordance with experimental data, and all indicators are consistent with formation of the TiO_2 (II) at 7.5 GPa and 1,000°C.

We used the following thermal expansion/contraction values (Ahrens, 1995) for our estimates of possible overpressure within the inclusion vessel:

Supplementary Table1

Thermal Expansion and Bulk Modulus Coefficients.(from Mineral Physics and Crystallography AGU Reference Shelf 2: Ahrens, 1995).

Mineral	T range (K)	a_o (10^{-6})
Picochromite	293-1473	16.5
Rutile	298-1883	28.9
Tremolite	297-973	31
Apatite	297-	34

Bulk Modulus

Mineral	Ks = adiabatic bulk modulus (Gpa)
Apatite	212.3
Chromite	203.3
Rutile	215.5
Amphibole	87-93

Bulk modulus describes which confining pressure is required to reduce the volume of a phase.

Of course, we cannot completely exclude the possibility that the apatite was a UHP phase (tuite) originally that also transformed back during cooling to simple apatite, and the pressures were higher than we estimate.Although, we observed no features of back transformation in the apatite, it is possible that such defects, if they existed, could have been healed completely by annealing during the uplift phase.

During exhumation, all phases would have slowly cooled with the thermal contraction of the inclusions being greater than the host chromite by virtue of their larger a_o (thermal expansion coefficient) (Supplementary Table 1). However, this would be modulated during uplift by the adiabatic bulk modulus (Ks) which is large for all of the observed phases except amphibole, which would expand slightly faster than the host, meaning that the internal pressure would have been maintained within the pressure vessel during exhumation.

Supplementary References

Ahrens, T. J., 1995. Mineral Physics and Crystallography: A Handbook of Physical Constants, vol. 2, American Geophysical Union, AGU Reference Shelf. doi.org/10.1029/RF002

Wirth, R., 2004. Focused Ion Beam (FIB): A novel technology for advanced application of micro- and nanoanalysis in geosciences and applied mineralogy. European Journal of Mineralogy 16, 863-876.doi.org10.1127/0935-1221/2004/0016-0863

Wirth, R., 2009. Focused Ion Beam (FIB) combined with SEM and TEM: Advanced analytical tools for studies of chemical composition, microstructure and crystal structure in geomaterials on a nanometre scale. Chemical Geology 261, 217-229. doi.org/10.1016/j.chemgeo.2008.05.019